Published in final edited form as:

ACS Catal. 2020 September 4; 10(17): 10229–10242. doi:10.1021/acscatal.0c02381.

Editing Domain Motions Preorganize the Synthetic Active Site of Prolyl-tRNA Synthetase

Quin H. Hu[1], **Murphi T. Williams**[1], **Irina Shulgina**[2], **Carl J. Fossum**[1], **Katelyn M. Weeks**[1], **Lauren M. Adams**[1], **Clorice R. Reinhardt**[1], **Karin Musier-Forsyth**[2,*], **Sanchita Hati**[1,*], **Sudeep Bhattacharyya**[1,*]

[1]Department of Chemistry and Biochemistry, University of Wisconsin-Eau Claire, WI, 54701, USA

[2]Department of Chemistry and Biochemistry and Center for RNA Biology, The Ohio State University, Columbus, OH, 43210, USA

Abstract

Prolyl-tRNA synthetases (ProRSs) catalyze the covalent attachment of proline onto cognate tRNAs, an indispensable step for protein synthesis in all living organisms. ProRSs are modular enzymes and the "prokaryotic-like" ProRSs are distinguished from "eukaryotic-like" ProRSs by the presence of an editing domain (INS) inserted between motifs 2 and 3 of the main catalytic domain. Earlier studies suggested the presence of coupled-domain dynamics could contribute to catalysis; however, the role that the distal, highly mobile INS domain plays in catalysis at the synthetic active site is not completely understood. In the present study, a combination of theoretical and experimental approaches has been used to elucidate the precise role of INS domain dynamics. Quantum mechanical/molecular mechanical simulations were carried out to model catalytic Pro-AMP formation by *Enterococcus faecalis* ProRS. The energetics of the adenylate formation by the wild-type enzyme was computed and contrasted with variants containing active site mutations, as well as a deletion mutant lacking the INS domain. The combined results revealed that two distinct types of dynamics contribute to the enzyme's catalytic power. One set of motions is intrinsic to the INS domain and leads to conformational preorganization that is essential for catalysis. A second type of motion, stemming from the electrostatic reorganization of active site residues, impacts the height and width of the energy profile and has a critical role in fine tuning the substrate orientation to facilitate reactive collisions. Thus, motions in a distal domain can preorganize the active site of an enzyme to optimize catalysis.

Graphical Abstract

*Corresponding authors K.M.-F.: musier-forsyth.1@osu.edu, S.H.: hatis@uwec.edu, S.B.: bhattas@uwec.edu.

ASSOCIATED CONTENT

Supporting Information

Additional information including primers used for making the mutant variants of Ec ProRS, key hydrogen bonding interactions at the transition state, hydrogen bonding interactions at the interface of INS and catalytic domain during the precursor complex formation, the RMSDs of the proline binding loop (PBL: residues: 199-206) based on 2-ns MD simulation data of the adenylation reaction, and the twin plots of populations vs. reaction coordinate for the propagated Umbrella sampling simulations to assess convergence will be made available free of charge via the Internet at http://pubs.acs.org.

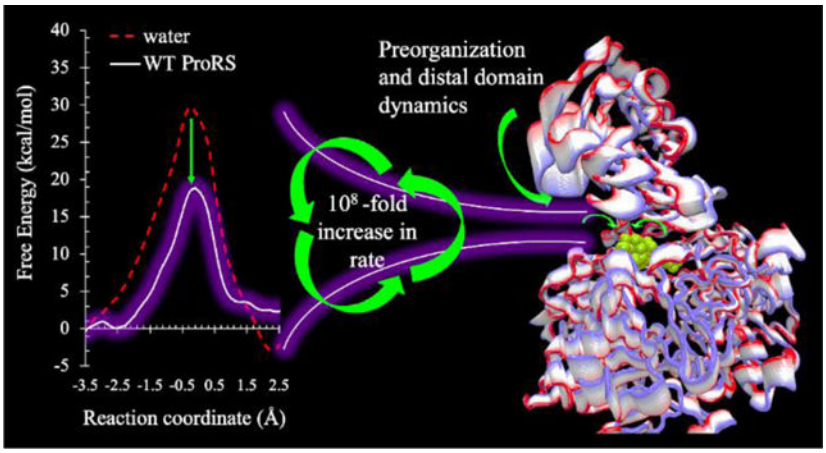

Keywords

Aminoacyl tRNA synthetase; coupled-domain motions; enzyme catalysis simulations; preorganization; protein dynamics; quantum mechanical/molecular mechanical simulations; reorganization

INTRODUCTION

Aminoacyl-tRNA synthetases (AARSs) are a family of enzymes that catalyze the covalent attachment of a specific amino acid onto the 3′-end of its cognate transfer ribonucleic acid (tRNA). This process is an indispensable step in genetic code translation, where the twenty canonical amino acids and their respective AARSs produce the aminoacyl-tRNA or charged tRNA for protein synthesis.[1–2] The aminoacylation of tRNA by AARSs is catalyzed by a two-step reaction. In the first step, an amino acid (AA) is activated in the presence of adenosine triphosphate (ATP) to form an enzyme-bound aminoacyl-adenylate with the release of pyrophosphate (PP_i) (eq. 1). The second step is the transfer of the activated amino acid to its cognate tRNA (eq. 2).[3–4]

$$\mathrm{AARS} + \mathrm{AA} + \mathrm{ATP} \rightleftharpoons \mathrm{AARS} \cdot (\mathrm{AA}{-}\mathrm{AMP}) + \mathrm{PP_i} \tag{1}$$

$$\mathrm{AARS} \cdot (\mathrm{AA} - \mathrm{AMP}) + \mathrm{tRNA}^{\mathrm{AA}} \rightarrow \mathrm{AA} - \mathrm{tRNA}^{\mathrm{AA}} + \mathrm{AARS} + \mathrm{AMP} \tag{2}$$

AARSs face the challenge of accurately identifying the specific amino acid through distinguishing similar sizes and chemical structures of amino acid side chains. In response, proofreading and/or editing mechanisms evolved in these enzymes to prevent and/or correct misacylation of tRNAs with noncognate amino acids.[5] Prolyl-tRNA synthetases (ProRSs) belong to the AARS family that catalyze the covalent attachment of proline to its cognate $\mathrm{tRNA}^{\mathrm{Pro}}$ through covalent bond formation between an oxygen of the proline carboxylate and the α phosphate of the ATP. In many organisms, ProRSs have been found to misactivate alanine and cysteine.[6–8] ProRSs in the “prokaryotic-like” group, consisting of prokaryotic and putative eukaryotic mitochondrial enzymes,[7] have developed a post-transfer editing

mechanism involving an insertion domain (INS, ~180 amino acids) located between the conserved motifs 2 and 3, which functions to hydrolyze Ala-tRNA^{Pro}.[9–10] In contrast, the "eukaryotic-like" ProRSs, consisting of eukarya, archaea and a few bacteria, do not possess the INS domain.[7] In some cases, a homologous free-standing editing domain is encoded and appears to function as the post-transfer editing domain in "eukaryotic-like" ProRSs.[11]

Earlier studies have focused on uncovering the molecular mechanism of the post-transfer editing reaction catalyzed by the INS domain,[9, 12–13] but the role of the INS domain in Pro-AMP formation and tRNA aminoacylation remains only partially understood. The residues of the INS domain do not participate directly in the aminoacylation reaction and are not adjacent to the active site. Additionally, circular dichroism measurements demonstrated that the deletion of the INS domain has no significant effect on the overall fold of the deletion mutant.[5] However, in *Escherichia coli* (Ec) ProRS, the INS domain (residues 232–394) was found to significantly impact amino acid binding and activation; the deletion of the INS domain resulted in a significant change in the efficiency of substrate binding resulting in a 200-fold increase in the K_M. Furthermore, the overall proline activation efficiency was reduced by ~1200-fold relative to that of the wild-type (WT) enzyme.[5] Previous studies have also shown that the covalent connectivity and coupled-domain dynamics between the INS and the catalytic domain are important for Ec ProRS function.[11, 14] However, the molecular mechanism by which the INS domain affects catalysis is still unclear.

We hypothesize that the INS domain may play an indirect role in the aminoacyl-adenylate formation reaction that is related to its intrinsic dynamics. To explore this hypothesis, the INS domain, the entire protein matrix, and a number of catalytic residues were probed using a combination of theory and experiment. The energetics of the Pro-AMP formation were determined using hybrid quantum mechanical/molecular mechanical (QM/MM) simulations and validated by site-directed mutagenesis and enzyme kinetics. The interplay of dynamics and electronic effects were probed in detail and the role of various types of motions and their relation to energetics were explored. Taken together, these studies provide new insights into how motion of a distal protein domain can impact catalysis at an enzyme's active site.

MATERIALS AND METHODS

Materials.

Primers for site-directed mutagenesis and polymerase chain reaction were purchased from Integrated DNA Technologies, Coralville, IA.

Enzyme Preparation.

All experimental kinetic studies were conducted with Ec ProRS as it possesses considerable sequence identity (56%) to *Enterococcus faecium* (Ef) ProRS. Besides the full-length WT enzyme, a truncated enzyme (constructed by the deletion of the INS domain, hereafter termed as ΔINS) and a number of active site mutants were prepared. Plasmids encoding E111A, E111D, R140A, R151A, R450A, and R450D (the corresponding residue is R447 in Ef ProRS) Ec ProRS were generated by site-directed mutagenesis of pCS-M1S[2] using primers listed in Table S1. DNA sequencing performed by the University of Wisconsin

Biotechnology Center, Madison confirmed successful mutagenesis. WT and mutant Ec ProRSs, tagged with six histidine residues (His_6) at the N-terminus, were overexpressed and purified as previously described.[15–16] Briefly, 0.1 mM isopropyl β-D-thiogalactoside was used to induce protein overexpression in Ec SG13009 (pREP4) competent cells for 4h at 37°C. Purification of histidine-tagged proteins was carried out using Talon cobalt affinity resin; proteins were eluted from the column with 100 mM imidazole and concentrations were initially determined by the Bio-Rad Protein Assay (Bio-Rad Laboratories).[17]

Enzyme Assays.

The ATP-PP_i exchange assay was performed at 37 °C according to the published method.[18] The concentrations of proline ranged from 0.025 – 2.0 mM. The Ec ProRS concentrations, as determined from active site titrations[19] were 100 nM and 1 μM for WT and mutant ProRS, respectively. Kinetic parameters were determined from Lineweaver-Burk plots [6, 20] and represent the average of at least 2 determinations.

Computational Setup.

All protein systems for QM/MM simulations were prepared starting with the X-ray crystallographic structure of Ef ProRS [PDB entry 2J3M ("open" state)][21], which contains the bound ATP and prolinol. The substrate proline was reconstructed to be in the zwitterionic form and introduced into the active site. The Mn^{2+} ions, which were used in place of Mg^{2+} ions for protein crystallization, were replaced with Mg^{2+} ions. The ΔINS enzyme was constructed by replacing INS residues 232–394 with a 16-residue $Gly_{12}Ser_4$ linker[5] generated with the Mutator plug-in of Visual Molecular Dynamics (VMD).[22] The mutants E111A, E111D, R140A, R151A, R447A, and R447D were constructed by using a script in VMD as well. All enzyme and aqueous systems were constructed using procedures described earlier.[23–26] Briefly, after obtaining the atomic coordinates from crystal structures, the hydrogen atoms were added using HBUILD utility of CHARMM.[27] The protonation state of all side chains was modeled at pH 7. All histidine residues were modeled as neutral. The protonation state of each histidine was judged based on the surrounding residues in the crystal structure, where potential hydrogen bonding was the primary consideration. The protonation state of N_ε and N_δ atoms of the imidazole moiety was further verified by computing the pK_a using Propka.[28–29] Only the substrates in the active site of chain A were kept for simulations. The active site-bound ATP and proline were solvated by placing the α-phosphorus of the active site-bound ATP of chain A as the origin in a sphere (radius of 60 Å) of explicit water. All residues outside the water sphere of 60 Å radius were truncated, and no special treatment was applied to the open valences of residues at the surface of the sphere. In the process of truncation, all residues of the enzyme subunit containing the active site was preserved and only the residues in the INS domain of the second subunit was removed. The solvated enzyme system was neutralized with additional Mg^{2+} ions placed randomly throughout the entire spherical region. The solvated system was equilibrated by 500 ps MD simulations.

Simulation Conditions.

Hybrid quantum/classical (QM/MM) simulations were carried out following simulation conditions described earlier.[23–24] The triphosphate group of the ATP and proline were

treated using self-consistent charge-density functional tight-binding (SCC-DFTB).[30–32] The remaining atoms of the system, including the entire enzyme and all water, were treated classically using the CHARMM27 all-atom force fields[33] with grid-based cross-term energy map corrections for protein backbone atoms[34] (Figure 1a). Unlike ATP hydrolysis, where Mg^{2+} ion is known to activate water, [35] the role played by the Mg^{2+} ions in the prolyl-adenylate formation is to stabilize the charges on phosphates. Since an explicit role in the bond breaking/forming process was ruled out, a fixed-charged model of Mg^{2+} ions was deemed to be sufficient in the present case. Therefore, Mg^{2+} ions were not included in the QM region. The link atom method was used to define the QM/MM boundary,[36] where a hydrogen-like atom was used to saturate the bond between the QM frontier atom C5′ of ATP and MM-treated atom C4′ of ATP shown in Figure 1b. Stochastic boundary conditions were employed to simulate the enzymatic-solvent interactions.[37] Water molecules of all systems were represented using the three-point-charge TIP3P model.[38] Bond lengths and bond angles of water molecules were constrained by the SHAKE algorithm.[39] Langevin dynamics were employed in the 48–60 Å region for the 60 Å spherical system, with increasing frictional forces as approaching the circumferential boundary.[40] An overall visual representation of the simulation conditions is shown in Figure 1. Non-bonded interactions were truncated using a switching function between 11 and 12 Å. In all molecular dynamics (MD) simulations, a time step of 1 fs was used in the leapfrog Verlet algorithm for integration.[41–42]

Umbrella Sampling-Guided Potential of Mean Force Calculation.

The adenylate formation reaction in each system was simulated using multiple-window adaptive-bias umbrella sampling techniques.[43] In this technique, the change in Gibbs free energy for each system was obtained as a potential of mean force (PMF)[44] along the reaction coordinate defined as

$$\xi(\text{Å}) = r_{\text{break}} - r_{\text{form}} \tag{3}$$

where r_{break} represents the bond breaking in the reaction and is $r_{\text{PA–O3A}}$, and r_{form}, the bond forming, is $r_{\text{OTX–PA}}$, both representing internuclear distances shown in Figure 1b. The range of the reaction coordinate was chosen to be from –3.0 Å to +3.0 Å, which was divided into 20 individual simulation segments of 0.3 Å. In each segment, sampling was done by applying a harmonic biasing potential, which acts as a restraining force centered at the mid-point (ξ_o) of that bin. Biased conformations were sampled within the range of $\xi_o \pm 0.5$ Å to allow sufficient overlap between neighboring bins. Simulations in each bin was propagated by taking two random conformations and observing the conformational distributions of the continued parallel simulations (Figure S1). The convergence was judged manually from the occurrence of the Gaussian distributions of the propagated simulations. A total of 2 ns of configurations along ξ were sampled. The combined sampling of the entire reaction coordinate of each parallel simulated system was then collected and analyzed by the weighted histogram analysis method (WHAM)[45] to produce a plot of the reaction coordinate ξ (Å) versus PMF (kcal/mol) to obtain the unbiased free energy profile for the reaction. The

overall barrier height in the iterated PMFs differed by less than 0.5 kcal/mol indicating convergence.

Measurement of Active Site Volume.

The active site volume was measured using the computational program POCASA.[46] Briefly, a 3D grid system was first generated with heavy atoms of protein using their van der Waals radii. Next, using a probe sphere to roll over the protein surface, a "probe surface" was generated. The generated probe surface was compared to the protein surface to detect binding pockets. For the WT and mutants, the % change in the active site volume were calculated for the precursor complex (PC) and successor complex (SC) states. In each case, the coordinates of protein atoms were prepared by removing ions, solvent, ATP, and proline and the volume of the active site was averaged on five conformations. The estimated errors of the calculations were obtained from the average value of the standard deviations of these measurements.

Essential dynamic analysis (EDA).

Essential dynamics[47] of the protein was analyzed using the program CARMA.[48] The procedure involves the calculation of principal component of motions as discussed earlier.[11] Briefly, the overall translational and rotational motions was removed and a modified trajectory was prepared by retaining the information of only C_α atoms' fluctuations. The principal components (or modes) of the motion were obtained as eigenvectors by diagonalizing the covariance matrix computed for C_α atoms. Based on the projections of the backbone fluctuations along the first three principal components,[48] the conformations were clustered into groups. The most populated cluster (highest number of frames per unit of displacement) was used to calculate the backbone displacement, which represents the predominant backbone flexibility[49] of the enzyme.

RESULTS AND DISCUSSION

The role of a protein matrix on catalysis includes electronic and dynamic effects as well as other structural and proton transfer effects.[50–54] The electronic effect is observed in the electrostatic response of the active site induced by the changing charge distribution during the course of a reaction.[55–57] The dynamic effects are manifested through protein motions of diverse timescales assisting substrate binding and catalytic rate enhancements.[50, 53–54, 58–66] Here, we studied the combined electronic and dynamic effects of the protein matrix on catalytic Pro-AMP formation (eq. 1) by bacterial ProRSs. The simulations were performed using SCC-DFTB/MM method, which has been previously validated by Hou et al. for a monomethylphosphate ester hydrolysis reaction.[67] In their study, the computed activation barrier was within 1–3 kcal/mol of the experimental results. A detailed analysis of the structural and dynamical changes allowed us to tie together the role of enzyme dynamics and charge stabilization on the overall catalytic process.

Wild-type Ef ProRS.

As for all class II ARSs, the synthetic active site of Ef ProRS, whose crystal structure has been determined in complex with ATP and a proline analog to 2.3 Å resolution (PDB code:

2J3M),[21] is located in the antiparallel β-sheet fold of the catalytic domain and contains consensus motifs 1, 2, and 3 (Figure 2). The editing active site is a distinct domain of the enzyme, inserted between motifs 2 and 3 of the synthetic active site. Following an equilibration step outlined in the methods section, the dynamically equilibrated synthetic active site shows that the ATP molecule forms a 'U'-shaped conformation (Figure 2), which is another conserved feature of class II ARSs. Analysis of the active site surface further reveals that electrostatic interactions play a significant role in binding; ATP and proline are tightly bound in the crevice formed by several charged/polar residues. Three arginine residues, namely R140, R151, and R447, form strong interactions with the negatively charged phosphate groups of ATP (Figure 2). Additionally, the ATP coordinates with two Mg^{2+} ions. Deep in the active site cavity, a π-stacking interaction between F155 and the adenine group of ATP is also observed (Figure 2).

Precursor complex (PC).—Following the umbrella sampling-guided simulation, the free energy profile for the WT enzyme exhibited a shallow (~1 kcal/mol) but well-formed free energy well at a reaction coordinate (ξ) of –2.5 Å (Table 1, Figure 3). During the formation of the PC, the carboxylate of the zwitterionic proline was found to be pointing towards the α-phosphate of ATP poised for a nucleophilic attack (Figure 4, top panel). Notably, R140 interacts with both the α-phosphate and the proline carboxylate group indicating that R140 plays a key role in facilitating the nucleophilic attack. The other two arginines, R151 and R447, interact with the γ-phosphate. The significantly bent shape of the ATP molecule is maintained throughout the simulation, amidst extensive hydrogen bonding interactions between the three arginine residues with oxygens from the three phosphate groups. The amide protons of proline are stabilized by nearby residues, T109 and E111. In addition, a strongly bonded water molecule is located near the proline and forms a hydrogen bonding network with T109, proline, and E111 (Figure 4).

Transition state (TS).—The TS in the WT enzyme occurs at $\xi = -0.1$ Å indicating that the breaking and forming bonds are about equal in length. The Gibbs free energy of activation ($\Delta_r^{\ddagger} G^{o}$) was calculated to be ~ 18 kcal/mol (Table 1, Figure 3). This activation barrier is within 1 kcal/mol of the experimentally determined rate constant k_{cat}, which corresponds to an activation barrier of 17 kcal/mol.[25]

The equilibrated conformation of the TS further showed that the α-phosphorous forms a trigonal bipyramidal structure (Figure 4, middle panel); one of the oxygen atoms of the proline carboxylate group occupies an axial position, while the other axial position is occupied by the oxygen bridging the β-phosphate. The penta-coordination of phosphorous in the TS is a common observation in enzymatic phosphate-transfer reactions.[68] The TS geometry shows that the central phosphorus atom has a trigonal plane consisting of 3 shorter (~1.5 Å) equatorial bonds with two longer axial (~1.8 Å) bonds perpendicular to the plane. The dissimilar bond distances are indicative of a sp^2 type of hybridization of the central phosphorous, which according to previous density functional theory-based studies, is due to the poor contribution of the d-orbitals to the molecular orbitals formed during the TS.[69–70]

The shape of the ATP molecule remained significantly bent amidst extensive hydrogen bonding interactions between three arginine residues and phosphate oxygens (Table S2). R140 plays a significant role in stabilizing the TS as its guanidium group is involved in strong hydrogen bonding with the α-phosphate of ATP as well as the carboxylate of the proline (Table S2). Significant interactions are also present between R151/R447 and the γ-phosphate oxygens of the ATP. Visual analysis of the trajectory of the TS revealed that the zwitterionic proline, although advanced closer towards the α-phosphate continued to interact with T109 and E111. A water molecule is retained by the same hydrogen bonding network as in the PC (Figure 4).

Successor complex (SC).—The computed PMF in the WT enzyme, generated a plateau region in the SC around ξ = 1.3 Å (Table 1). A further decrease in energy of ~1 kcal/mol was observed beyond this point with the formation of a second plateau region at ~1.9 Å (Figure 3). The reaction in the WT enzyme environment is endergonic, with a computed Gibbs free energy of reaction ($\Delta_r G^o$) of ~ 2.6 kcal/mol. The diphosphate drifted further away from Pro-AMP and continued to interact with R447 and R151 (Figure 4, bottom panel). Pro-AMP is stabilized by a number of electrostatic interactions. Near the central part of Pro-AMP, the newly formed phosphoester moiety is hydrogen bonded to the guanidinium group of R140. On the proline end of the molecule, the hydrogen bonding network involving T109 (hydroxyl group), proline (amide group) and E111 (carboxylate group) is found to be preserved.

Enzyme-free Condition (Aqueous) and ΔINS Ef ProRS.

The PMF of the prolyl-adenylate formation in an aqueous, enzyme-free system did not exhibit a discernible PC (Figure 5a), consistent with the absence of active site interactions identified in the PC of the WT enzyme. The absence of an enzyme matrix is most prominent in the TS; the computed $\Delta_r^{\ddagger} G^o$ was ~30 kcal/mol (Table 1 and Figure 5a), which is 12 kcal/mol higher than what is observed for the WT enzyme. This finding indicates that Pro-AMP formation in the enzyme-free system is kinetically inert. Compared to the WT enzyme, the PMF shows a much broader energy profile. Additionally, the reaction is exergonic in water, with a $\Delta_r G^o$ of −2.9 kcal/mol (Table 1, Figure 5a). Delayed formation of a stable SC was observed for the aqueous case with a ξ of ~2.3 Å (Table 1, Figure 5a).

The deletion mutant (ΔINS) lacking the complete INS domain (residues 220–400) is also observed to have a high activation barrier ($\Delta_r^{\ddagger} G^o$ = 22.4 kcal/mol) (Table 1). A stable SC was located at ξ = ~1.9 Å (Table 1, Figure 5a). In contrast to the full-length enzyme, the reaction is found to be exergonic with a $\Delta_r G^o$ of −3.7 kcal/mol. The exergonicity for the ΔINS Ef ProRS is similar to the aqueous system indicating that the products (PP_i and Pro-AMP) are stabilized by solvation in both cases.

E111A and E111D Ef ProRS.

Mutation of the glutamate at position 111 to alanine appears to have a destabilizing effect as the PMF for E111A does not show a well-formed PC (grey line, Figure 5b), which confirms that the key role of this residue is in stabilizing the PC in the native state. In contrast, upon

E111D mutation, a successful recovery of the PC formation was accomplished (dotted line, Figure 5b). However, large activation barriers (29–32 kcal/mol) were observed for both mutants (Table 1, Figure 5b) indicating that the enzyme will likely be functionally inactive. The endergonic nature was retained for both mutants, with a much larger $\Delta_r G^o$ (Table 1) indicating that SC will be much less stabilized.

R140A and R151A Ef ProRS.

Mutation of R140 and R151 are predicted to have a severe impact on the catalysis. In the WT enzyme, R140 bridges the carboxylate and the α-phosphate acting as a facilitator of the nucleophilic attack, while R151 forms interactions with the γ- phosphate in the TS. For both mutants, no discernible PC was observed in the energy profiles (Figure 5c). The impact of the lack of electrostatic interactions was most pronounced in the TS; a functionally inactive enzyme is evident from the very high $\Delta_r^{\ddagger} G^o$ values of 34 and 38 kcal/mol, for R140A and R151A Ef ProRS, respectively.

R447A and R447D Ef ProRS.

The R447A mutant exhibits a PMF with a $\Delta_r^{\ddagger} G^o$ value 2 kcal/mol higher than WT. The PMF suggests a delayed formation of the SC for this mutant with a of ~2.5 Å (Table 1), and in contrast to WT, the reaction was exothermic with a $\Delta_r G^o$ of −1.5 kcal/mol (Table 1, Figure 5d). Therefore, based on the computed PMF, R447A mutant is predicted to be active but less efficient than the WT enzyme due to the charge neutralization.

In contrast, a large Gibbs free energy of activation ($\Delta_r^{\ddagger} G^o$ = 29.1 kcal/mol) was observed in the computed PMF of the R447D mutant. Based on the structural analysis of the WT enzyme, R447 was observed to interact with the γ-phosphate in the TS. Therefore, the destabilization of the TS in the R447D mutant is due to the reversal of electrostatic charges on the side chain, which resulted in strong repulsion between the γ-phosphate and carboxylate of the aspartic acid.

Kinetic Studies of the Prolyl-adenylate Formation.

WT Ec ProRS (a close homolog of Ef ProRS) and the six mutant enzymes, namely, E111A, E111D, R140A, R151A, R450A, and R450D, were examined for their catalytic efficiencies in Pro-AMP formation. As mentioned earlier, R450 is the residue that corresponds to R447 in Ef ProRS. Using the ATP-PP_i exchange reaction, we found that all of mutations have a significant impact on catalysis (Table 2). The proline activation efficiency (k_{cat}/K_M) of E111D and R450A was reduced by 300- and 500-fold, respectively, similar to the ΔINS variant. No activity was detected for E111A, R140A, R151A, or R450D mutants. The decrease in catalytic efficiencies or loss of enzyme activity suggested that these four charged residues are critical for proline activation. As evident from Figure 4, these residues are involved in anchoring the substrates in proper orientation and stabilizing TS in the WT enzyme. The neutralization of their charges or charge reversal prevents the required interactions needed to bind substrates or stabilize TS and SC. Among the three arginines, mutations of R140 and R151 were found to have a greater impact on the catalysis. As

supported by hydrogen bonding analysis, both residues strongly interact with the three phosphates of ATP in the TS (middle panel of Figure 4 and Table S2), demonstrating their roles in TS stabilization. Furthermore, they also interact with PP_i and Pro-AMP during product formation (Figure 4, bottom panel) and hence are likely to play a role in PP_i release. Overall, the results of enzyme kinetics are consistent with the computational findings.

Conformational Change during Catalysis.

In a recent study of Ec ProRS in the absence of bound substrates, we observed a large conformational change of the INS domain in a 70-ns MD simulation.[71] Using EDA,[47] we observed a principal mode of motion of the INS domain during the 'closed' to 'open' transition.[71] Our focus in the present study was to detect whether a similar conformational change also occurs for the INS domain during the adenylate synthesis reaction catalyzed by Ef ProRS. For all the full-length proteins investigated (WT and six mutants), the INS domain moves towards the catalytic domain during catalysis (Figure 6a). The comparison of INS domain movement for WT and mutants was further scrutinized by performing EDA and computing the backbone displacements that occurs along the first three principal components of motions. The relevance of the motions is discussed below in the broader context of catalysis. In each case of EDA, the displacement is calculated with respect to the starting conformation, for four states: (1) the apo-enzyme lacking both substrates (ATP and proline); (2) the substrate-bound PC; (3) during the entire course of catalysis; (4) the product-bound SC. In each of these states, the RMSDs, averaged over all backbone C_α atoms, were calculated (Table 3).

There was a significant reduction in the displacement (by 0.8 − 2.0 Å) going from the apo state to the PC state (Table 3) indicating substrate binding-induced changes in the overall dynamics of the active site. This is consistent with the strong interaction between the ATP and several residues at the synthetic active site (see Figure 4). The pattern was maintained for all proteins alike indicating that the motion is intrinsic to the protein. Interestingly, the backbone fluctuations of the WT enzyme are higher during catalysis, than the SC state (Table 3). The occurrence of a compact (i.e. closely packed) structure at the completion of the reaction may have a functional significance. For example, the product of the first step is an intermediate in overall tRNA aminoacylation; the compact structure may slow down Pro-AMP release from the active site.

Preorganization and Reorganization in Ef ProRS.

An enzyme is known to employ two types of motions in catalysis: preorganization and reorganization.[53, 59–60, 66, 72–73] Preorganization encompasses the movement of protein segments including distant domains forming an active site that favors substrate binding in proper orientation and proximity. These slow time-scale dynamics produce an active site that provides thermodynamic stability to the PC and the TS.[59–60] In contrast, reorganization involves faster movement of active site atoms facilitating reactive collisions between substrates thereby decreasing the activation barrier. [53, 58]

Conformational Motion of the INS Domain and Preorganization.—The INS domain is located proximal to the synthetic active site in the WT enzyme and full-length

mutants (Figure 6a). Although the region near the γ-phosphate of ATP is wide open, the proline-binding pocket is quite compact due to the presence of the PBL (residues 199–206) (Figure 6a). The INS domain interacts with the PBL through a well-formed hydrogen bonding network consisting of polar residues and several water molecules.[11] This includes the conserved "GED" motif (residues 217–219) at the inter-domain interface, N232, and K306.[11] Two strong hydrogen bonding interactions were noted: N232(INS domain) - E209(PBL) and K306(INS domain) - D198(PBL). These interactions were present in all full-length mutants during the formation of the PC (Table S3) and thus the presence of the INS domain creates a compact synthetic active site that presumably restricts solvent accessibility from one end (Figure 6b). This compact active site facilitates tighter substrate binding, which is demonstrated by the 200-fold decrease in K_M for the full-length compared to the deletion mutant.[5] In contrast to the full-length enzyme, the active site is open and readily exposed to the solvent in the ΔINS mutant (Figure 6c). The PBL was found to be dangling above the active site indicating that proline binding was partially impaired because of the deletion of the INS domain. This is also evident in the higher value of the RMSD of the PBL during catalysis for the ΔINS mutant (Table S4).

Changes in the width of the open end of the active site cleft were measured by taking the distance between the alpha-helix (318 to 327, subunit A) of the INS domain and the loop region (98 to 102, subunit B) of the catalytic domain (Figs. 6b and 6d). As evident in Table 4, the open end of the active site cleft shrinks as the reaction progresses in all enzyme systems. As discussed earlier, the active site near the proline is closed (Figs. 6a and 6b), thus the INS domain dynamics is likely to make the active site more compact facilitating contacts between the two substrates. This is evident from the change in volume of the active site during catalysis, measured using the POCASA program.[46] The analysis of the active site volume suggests that all but R447A (lacking the arginine that provides electrostatic stabilization of the γ-phosphate) mutants exhibit a decrease in active site volume during transition from PC to SC states (Table 4). The observed compactness upon substrate binding is also consistent with the sharp decrease in RMSD as discussed earlier (Table 3).

The role of INS domain in substrate binding is also revealed in the PMF profile of ΔINS (Figure 5a), where the formation of PC occurs at $\xi = -3.0$ Å (Table 1). Recall that the PC occurs at −2.5 Å in WT enzyme, but at a higher negative value (< −3.5 Å) in aqueous (enzyme-free) system. Therefore, the lack of INS domain causes an impairment of substrate binding, which otherwise promoted preorganization in the WT enzyme. This theoretical observation is also aligned with the experimentally observed higher K_M for the ΔINS mutant.[5] In summary, the analysis of the conformational change and energetics portrays a role of INS in preorganizing the active site during Pro-AMP formation.

Active site Reorganization.—Fast reorganizational motion of active site atoms are believed to be responsible for decreasing the distance between reacting molecules in enzymes thereby favoring catalysis.[70] In order to probe the protein motion along the bond-breaking and bond-forming direction during the adenylate formation reaction, a distance variation plot was generated by choosing the two ends of the active site. On one end of the active site, E111 that interacts with the proline amino group was selected. On the other end, R151 was chosen as it interacts with the γ-phosphorous of the ATP. In particular, the

distance between E111(C_α) and R151(C_α) vs. the reaction coordinate, defined as ξ in eq. 3, was plotted for the catalytic reaction using a 2 ns MD simulation data. For the WT, a compressing motion, along the direction of the nucleophilic attack by the proline carboxylate to the phosphate, was observed. In particular, there was a gradual decrease in the E111(C_α) - R151(C_α) distance, which is ~ 2 Å as the reaction passes through the transition state (Figure 7). The distance gradually increases by the same amount after the conclusion of the reaction. The decrease is slightly less (~ 1.5 Å) for ΔINS ProRS, but the pattern was maintained. However, the pattern was completely lost for E111 and R151 mutants, demonstrating that these residues are actively involved in the active site reorganization. Other mutants also exhibited patterns indicative of impaired reorganization dynamics (Figure 7). In summary, this analysis demonstrated the existence of compressing motion in the synthetic active site of WT Ef ProRS, which likely facilitates the nucleophilic attack of the ATP by the proline.

Dynamics and Reorganization Energy.—Pro-AMP formation is an SN_2 type of reaction. It can also be treated as an enzyme-catalyzed group transfer reaction, wherein an adenosine monophosphate (AMP) group is covalently attached to proline, resulting in the release of PP_i (Figure 8a). Following the original theoretical framework of Marcus[74–77] and later modified by Warshel,[78] the Gibbs free energy of activation ($\Delta_r^{\ddagger} G^o$) can be expressed as a quadratic function of the Gibbs free energy of a reaction ($\Delta_r G^o$):

$$\Delta_r^{\ddagger} G^o = \frac{\left(\Delta_r G^o + \lambda\right)^2}{4\lambda} \ldots \quad (4)$$

where, λ is the reorganization energy, defined as the hypothetical amount of energy needed to deform the potential energy surface (PES) of the reactant (i.e. the PC) to become that of the product (i.e. the SC). Thus, λ represents the work done by the enzyme[57] to respond to the change in charge distribution during the reaction. The reactant and product free energy curves are depicted as two parabolas in Figure 8b, where the x-axis represents the change in the nuclear coordinate and the y-axis is the Gibbs free energy. We note that eq. 4 is the result of a harmonic approximation of the change in Gibbs free energy to that of the nuclear coordinates. Therefore, for an enzyme-catalyzed group transfer reaction, the free energy change can still be considered as a quadratic function of the nuclear coordinate, which is a combination of bond vibrational coordinates of participating atoms and solvent dipoles within the active site.[79]

A plot of $\Delta_r^{\ddagger} G^o$ vs. $\Delta_r G^o$ was generated for Pro-AMP formation by WT and mutant variants (Figure 8c). The energetics of the adenylate formation reaction by the mutants fitted nicely to a quadratic equation. A non-linear trend, as expected for a group transfer reaction that follows the Marcus model,[80] was obtained for the single-point mutants as well as for the ΔINS variant (black triangles in Figure 8c). From the fitted curve, a reorganization energy value of 90 kcal/mol was computed for mutants according to eq. 4. The free energy values (i.e. $\Delta_r G^o$ and $\Delta_r^{\ddagger} G^o$) in the aqueous system (i.e. enzyme-free, red triangle in Figure 8c) and WT (Figure 8c, green triangle) did not fall on this trendline and eq. 4 yielded

reorganization energies of 117 and 61 kcal/mol (Figure 8c), respectively. Thus, compared to the WT enzyme, the reorganization energy increased by 30 kcal/mol for the mutants. This indicates a substantially reduced catalytic power due to active site mutations or the INS domain deletion, which also resulted in elevated activation free energy barriers (Table 1). The higher reorganization energy for the enzyme-free system compared to the WT enzyme is indicative of the native active site's catalytic power.[57] Since the width of the PMFs are different in the WT and in the enzyme-free system, the work term to bring the reactants together can partly explain the difference in the computed reorganization energy as described by Tu et al. in the context of proton transfer in carbonic anhydrase.[81]

Dynamics and Catalysis.—The conformational change observed for INS domain (Figure 9a) is completely consistent with the observed long-duration (70 ns) MD simulations with Ec ProRS.[71] The EDA-derived displacements depicted in the first principal mode (Figure 9b) demonstrate that the entire INS domain moving towards the catalytic domain during catalysis. Although the INS domain motion was present in WT ProRS and all full-length mutants, the missing electrostatic interaction in the synthetic active site was found to impair the motion within the active site (Figure 7). A comparison plot of the PMF width and the displacement of the protein C_α atoms (with respect to the starting conformation) during catalysis is shown in Figure 9c. The displacement of the entire protein backbone, as well as a region within 20 Å of the proline, were used in the analysis. Compared to the WT enzyme, all mutants had larger PMF width (Figure 9c, green diamonds) indicating larger nuclear displacement along the reaction coordinate (Figure 8b). These mutants also exhibited larger reorganization energies compared to WT ProRS (Figure 8c). Thus, the widening of PMFs for mutant variants is in full agreement with the increase in reorganization energy. Furthermore, Figure 9b demonstrates an inverse relationship between the backbone displacements and the width of the PMF. For example, the fluctuations in these mutants during catalysis were notably less for the active site C_α atoms (within 20 Å of the substrate). In summary, higher PMF width and lower backbone fluctuations corresponded to a higher reorganization energy for the adenylate formation reaction. This is consistent with the role of the enzyme to bring substrates in proximity and orient them to facilitate reactive collisions, thereby decreasing the width and height of the energy profile.

Analysis of water.—Being involved in the preorganization, the INS domain is expected to restrict solvent accessibility into the active site of full-length enzymes. To examine this effect, the radial distribution function (RDF) around the phosphorous atom undergoing the nucleophilic attack (i.e. P_α) was plotted for a distance up to 10 Å for the WT and its mutants (Figure 10). Compared to WT, all mutants exhibited a larger presence of water, most prominently in ΔINS and R140A. The trend is also in agreement with the general concept that the presence of more mobile water molecules indicates less preorganization and hence correlate to a larger reorganization energy.[57] Taken together, the present study provides a deeper insight into how preorganization and reorganization dynamics influence the free energy landscape of enzyme catalysis.

CONCLUSIONS

Here, we used computational and experimental approaches to probe the role of intrinsic protein domain dynamics on enzyme catalysis by bacterial ProRS. The results revealed the role of preorganization and reorganization on Pro-AMP formation by Ef ProRS. INS/editing domain dynamics play a distinct role in the structural preorganization for effective catalysis. The swinging motion of the INS domain appears to be intrinsic to the folded protein and is present even in the absence of the substrates. The dynamics remained unaffected by mutations of charged residues in the active site. However, deletion of the INS domain had a significant impact on catalysis. The compact preorganized active site, observed in the full-length enzyme, consists of hydrogen bonding interactions between the PBL and INS residues. In the ΔINS mutant, the active site was partially exposed, and these interactions were missing resulting in a dangling PBL. Scrutiny of the active site in the PC suggests that the proximity of the two substrates were also not optimum and the computed PMF demonstrated a higher activation barrier implying the impact of the INS domain on kinetics.

One of the major findings of the present study is that the INS domain deletion and other single-point mutations produced an active site that follows characteristics of the Marcus model of group transfer reactions. The plot of $\Delta_r^{\ddagger} G^{o}$ vs. $\Delta_r G^{o}$ (Figure 8c) revealed that the favorability of the catalysis exhibited a quadratic relationship with the activation barrier, which is a characteristic of the Marcus model (eq. 4). There are only a few reports of enzymatic group transfer reactions that exhibit this relationship between the equilibrium and kinetic free energy differences.[80] The present study is the first report of this observation in an enzymatic adenylate formation reaction, involving transfer of an AMP group to an amino acid.

The catalytic power of an enzyme originates from the preorganized and reorganized electrostatics of its active site.[57, 60, 72–73] The present study established the combined role of the preorganizational motion of the distal INS domain (slow motion) and the reorganizational fluctuations of active site residues (fast motion) on catalysis. Loss of the preorganizational motion contributed by the INS domain diminishes the enzyme's catalytic power by approximately half. A similar loss of catalytic power was also observed for the single-point mutants that disrupted reorganizational dynamics. Although there was a reduced overall backbone displacement in the full-length mutants compared to WT enzyme, as evident from the EDA-derived motions, they exhibited a larger number of mobile water molecules and hence less preorganization in the active site during catalysis. This observation corresponds to a larger reorganization energy than the native active site. The combined effect of these dynamics in the WT enzyme contributes to a lowering of the activation barrier ($\Delta_r^{\ddagger} G^{o}$) by ~11 kcal/mol (Table 1), which translates into an ~ 10^8-fold rate-enhancement relative to aqueous solution.

In summary, the results of this study demonstrate that the catalytic power of a modular enzyme like bacterial ProRS originates from concerted preorganizatioal and reorganizational effects involving both electrostatics and dynamics. This observation reasserts that these two

effects are conjoined factors for the catalytic power of an enzyme and, as described by Marti et al.,[73] can be viewed as “two faces of the same coin”.

Supplementary Material

Refer to Web version on PubMed Central for supplementary material.

ACKNOWLEDGEMENTS

We thank Dr. Marina Bakhtina for critical reading of the manuscript and helpful comments. We acknowledge the computational support of the Blugold Supercomputing Cluster (BGSC) and the technical help from the Learning and Technology Center, of University of Wisconsin-Eau Claire. The authors greatly thank three anonymous reviewers for their constructive comments.

Funding

This work was supported in part by National Institute of Health [grant numbers R15 GM117510 (S.H. and S.B.) and RO1 GM113656 (K.M.-F.)], The Extreme Science and Engineering Discovery Environment (XSEDE) [grant number MCB110173 (S.H. and S.B.)], and by the Office of Research and Sponsored Programs of the University of Wisconsin-Eau Claire, Eau Claire, WI.

ABBREVIATIONS USED

AARS	aminoacyl-tRNA synthetase
EDA	Essential dynamics analysis
Ef	*Enterococcus faecium*
Ec	*Escherichia coli*
INS	insertion domain
MD	molecular dynamics
MM	molecular mechanical
PC	precursor complex
PMF	potentials of mean force
ProRS	prolyl-tRNA synthetase
QM	quantum mechanical
QM/MM	quantum mechanical/molecular mechanical
RMSD	root-mean-square-deviation
SCC-DFTB	self-consistent charge-density functional tight-binding
SC	successor complex
tRNA	transfer ribonucleic acid
TS	transition state

BIBLIOGRAPHY

1. Cusack S, Aminoacyl-tRNA Synthetases. Curr. Opin. Struct. Biol 1997, 7, 881–889. [PubMed: 9434910]
2. Chaliotis A; Vlastaridis P; Mossialos D; Ibba M; Becker HD; Stathopoulos C; Amoutzias GD, The Complex Evolutionary History of Aminoacyl-tRNA Synthetases. Nucleic Acids Res. 2017, 45, 1059–1068. [PubMed: 28180287]
3. Freist W, Mechanisms of Aminoacyl-tRNA Synthetases: a Critical Consideration of Recent Results. Biochemistry 1989, 28, 6787–6795. [PubMed: 2684265]
4. Francklyn CS, DNA Polymerases and Aminoacyl-tRNA Synthetases: Shared Mechanisms for Ensuring the Fidelity of Gene Expression. Biochemistry 2008, 47, 11695–11703. [PubMed: 18850722]
5. Hati S; Ziervogel B; Sternjohn J; Wong FC; Nagan MC; Rosen AE; Siliciano PG; Chihade JW; Musier-Forsyth K, Pre-transfer Editing by Class II Prolyl-tRNA Synthetase: Role of Aminoacylation Active Site in "Selective Release" of Noncognate Amino Acids. J. Biol. Chem 2006, 281, 27862–27872. [PubMed: 16864571]
6. Beuning PJ; Musier-Forsyth K, Hydrolytic Editing by a Class II Aminoacyl-tRNA Synthetase. Proc. Natl. Acad. Sci. U. S. A 2000, 97, 8916–8920. [PubMed: 10922054]
7. Beuning PJ; Musier-Forsyth K, Species-specific Differences in Amino Acid Editing by Class II Prolyl-tRNA Synthetase. J. Biol. Chem 2001, 276, 30779–30785. [PubMed: 11408489]
8. Ahel I; Stathopoulos C; Ambrogelly A; Sauerwald A; Toogood H; Hartsch T; Soll D, Cysteine Activation is An Inherent In Vitro Property of Prolyl-tRNA Synthetases. J. Biol. Chem 2002, 277, 34743–34748. [PubMed: 12130657]
9. Wong FC; Beuning PJ; Nagan M; Shiba K; Musier-Forsyth K, Functional Role of the Prokaryotic Proline-tRNA Synthetase Insertion Domain in Amino Acid Editing. Biochemistry 2002, 41, 7108–7115. [PubMed: 12033945]
10. Wong FC; Beuning PJ; Silvers C; Musier-Forsyth K, An Isolated Class II Aminoacyl-tRNA Synthetase Insertion Domain is Functional in Amino Acid Editing. J. Biol. Chem 2003, 278, 52857–52864. [PubMed: 14530268]
11. Sanford B; Cao B; Johnson JM; Zimmerman K; Strom AM; Mueller RM; Bhattacharyya S; Musier-Forsyth K; Hati S, Role of Coupled Dynamics in the Catalytic Activity of Prokaryotic-like Prolyl-tRNA Synthetases. Biochemistry 2012, 51, 2146–2156. [PubMed: 22356126]
12. Splan KE; Ignatov ME; Musier-Forsyth K, Transfer RNA Modulates the Editing Mechanism Used by Class II Prolyl-tRNA Synthetase. J. Biol. Chem 2008, 283, 7128–7134. [PubMed: 18180290]
13. Bartholow TG; Sanford BL; Cao B; Schmit HL; Johnson JM; Meitzner J; Bhattacharyya S; Musier-Forsyth K; Hati S, Strictly Conserved Lysine of Prolyl-tRNA Synthetase Editing Domain Facilitates Binding and Positioning of Misacylated $tRNA^{Pro}$. Biochemistry 2014, 53, 1059–1068. [PubMed: 24450765]
14. Strom AM; Fehling SC; Bhattacharyya S; Hati S, Probing the Global and Local Dynamics of Aminoacyl-tRNA Synthetases using All-atom and Coarse-grained Simulations. J. Mol. Model 2014, 20, 2245. [PubMed: 24810463]
15. Stehlin C; Heacock DH 2nd, Liu H; Musier-Forsyth K, Chemical Modification and Site-Directed Mutagenesis of the Single Cysteine in Motif 3 of Class II Escherichia Coli Prolyl-tRNA Synthetase. Biochemistry 1997, 36, 2932–2938. [PubMed: 9062123]
16. Burke B; Lipman RS; Shiba K; Musier-Forsyth K; Hou YM, Divergent Adaptation of tRNA Recognition by Methanococcus Jannaschii Prolyl-tRNA Synthetase. J. Biol. Chem 2001, 276, 20286–20291. [PubMed: 11342535]
17. Fersht AR, Demonstration of Two Active Sites on a Monomeric Aminoacyl-tRNA Synthetase. Possible Roles of Negative Cooperativity and Half-of-the-Sites Reactivity in Oligomeric Enzymes. Biochemistry 1975, 14, 5–12. [PubMed: 1109589]
18. Heacock D; Forsyth CJ; Shiba K; Musier-Forsyth K, Synthesis and aminoacyl-tRNA synthetase inhibitory activity of prolyl adenylate analogs. Bioorg. Chem 1996, 24, 273–289.

19. Fersht AR; Ashford JS; Bruton CJ; Jakes R; Koch GL; Hartley BS, Active Site Titration and Aminoacyl Adenylate Binding Stoichiometry of Aminoacyl-tRNA Synthetases. Biochemistry 1975, 14, 1–4. [PubMed: 1109585]
20. Lineweaver H; Burk D, The Determination of Enzyme Dissociation Constants. J. Am. Chem. Soc 1934, 56, 658–666.
21. Crepin T; Yaremchuk A; Tukalo M; Cusack S, Structures of two bacterial prolyl-tRNA synthetases with and without a cis-editing domain. Structure 2006, 14, 1511–1525. [PubMed: 17027500]
22. Humphrey W; Dalke A; Schulten K, VMD: Visual Molecular Dynamics. J. Mol. Graph 1996, 14, 33–38. [PubMed: 8744570]
23. Reinhardt CR; Hu QH; Bresnahan CG; Hati S; Bhattacharyya S, Cyclic Changes in Active Site Polarization and Dynamics Drive the 'Ping-pong' Kinetics in NRH:Quinone Oxidoreductase 2: An Insight from QM/MM Simulations. ACS Catal. 2018, 8, 12015–12029. [PubMed: 31583178]
24. Mueller RM; North MA; Yang C; Hati S; Bhattacharyya S, Interplay of Flavin's Redox States and Protein Dynamics: An Insight from QM/MM Simulations of Dihydronicotinamide Riboside Quinone Oxidoreductase 2. J. Phys. Chem. B 2011, 115, 3632–3641. [PubMed: 21410212]
25. Johnson JM; Sanford BL; Strom AM; Tadayon SN; Lehman BP; Zirbes AM; Bhattacharyya S; Musier-Forsyth K; Hati S, Multiple Pathways Promote Dynamical Coupling Between Catalytic Domains in Escherichia Coli Prolyl-tRNA Synthetase. Biochemistry 2013, 52, 4399–4412. [PubMed: 23731272]
26. Bresnahan CG; Reinhardt CR; Bartholow TG; Rumpel JP; North M; Bhattacharyya S, Effect of Stacking Interactions on the Thermodynamics and Kinetics of Lumiflavin: A Study with Improved Density Functionals and Density Functional Tight-Binding Protocol. J. Phys. Chem. A 2015, 119, 172–182. [PubMed: 25490119]
27. Brooks BR; Bruccoleri RE; Olafson BD; States DJ; Swaminathan S; Karplus M, CHARMM: A Program for Macromolecular Energy, Minimization, and Dynamics Calculations. J. Comput. Chem 1983, 4, 187–217.
28. Olsson MH, Protein Electrostatics and pKa Blind Predictions; Contribution from Empirical Predictions of Internal Ionizable Residues. Proteins 2011, 79, 3333–3345. [PubMed: 22072518]
29. Olsson MH; Sondergaard CR; Rostkowski M; Jensen JH, PROPKA3: Consistent Treatment of Internal and Surface Residues in Empirical pKa Predictions. J. Chem. Theory Comput 2011, 7, 525–537. [PubMed: 26596171]
30. Elstner M; Porezag D; Jungnickel G; Elstner J; Haugk M; Frauenheim T; Suhai S; Seifert G, Self-Consistent-Charge Density-Functional Tight-Binding Method for Simulations of Complex Materials Properties. Phys. Rev. B 1998, 58, 7260–7268.
31. Frauenheim T; Seifert G; Elstner M; Hajnal Z; Jungnickel G; Porezag D; Suhai S; Rcholz R, A Self-Consistent Charge Density-Functional Based Tight-Binding Method for Predictive Materials Simulations in Physics, Chemistry and Biology. Phys. Stat. Sol. B 2000, 217, 41–62.
32. Cui Q; Elstner M; Kaxiras E; Frauenheim T; Karplus M, A QM/MM Implementation of the Self-Consistent Charge Density Functional Tight Binding (SCC-DFTB) Method. J. Phys. Chem. B 2001, 105, 569–585.
33. MacKerell ADJ; Bashford D; Bellott M; Dunbrack RLJ; Evanseck JD; Field MJ; Fischer S; Gao J; Gou J; Ha S; Joseph-McCarthy D; Kuchnir L; Kuczera K; Lau FTK; Mattos C; Michnick S; Ngo T; Nguyen DT; Prodhom B; Reiher WEI; Roux B; Schelenkrich M; Smith JC; Stote R; Straub J; Watanbe M; Wiórkiewicz-Kuczera J; Yin D; Karplus M, All Atom Empirical Potential for Molecular Modeling and Dynamics Studies of Proteins. J. Phys. Chem. B 1998, 102, 3586–3616. [PubMed: 24889800]
34. Mackerell AD Jr.; Feig M; Brooks CL 3rd, Extending the Treatment of Backbone Energetics in Protein Force Fields: Limitations of Gas-phase Quantum Mechanics in Reproducing Protein Conformational Distributions in Molecular Dynamics Simulations. J. Comput. Chem 2004, 25, 1400–1415. [PubMed: 15185334]
35. Yang Y; Yu H; Cui Q, Extensive Conformational Transitions are Required to Turn on ATP Hydrolysis in Myosin. J. Mol. Biol 2008, 381, 1407–1420. [PubMed: 18619975]
36. Reuter N; Dejaegere A; Maigret B; Karplus M, Frontier Bonds in QM/MM Methods: A Comparison of Different Approaches. J. Phys. Chem. A 2000, 104, 1720–1735.

37. Brooks CLI; Karplus M, Deformable Stochastic Boundaries in Molecular Dynamics. J. Chem. Phys 1983, 79, 6312–6325.
38. Jorgensen WL; Chandrasekhar J; Madura JD; Impey RW; Klein ML, Comparison of Simple Potential Functions for Simulating Liquid Water. J. Chem. Phys 1983, 79, 926–935.
39. Ryckaert JP; Ciotti G; Berensden HJC, Numerical Integration of the Cartesian Equations of Motion of a System with Constraints: Molecular Dynamics of n-Alkanes. J. Comput. Phys 1977, 23, 327–341.
40. Bhattacharyya S; Ma S; Stankovich MT; Truhlar DG; Gao J, Potential of Mean Force Calculation for the Proton and Hydride Transfer Reactions Catalyzed by Medium-Chain Acyl-CoA Dehydrogenase: Effect of Mutations on Enzyme Catalysis. Biochemistry 2005, 44, 16549–16562. [PubMed: 16342946]
41. Verlet L, Computer "Experiments" on Classic Fluids. I. Thermodynamical Properties of Lennard-Jones Molecules. Phys. Rev 1967, 159, 98–103.
42. Hockney RW, The Potential Calculation and Some Applications. Methods Comput. Phys 1970, 9, 136–211.
43. Mills M; Andricioaei I, An Experimentally Guided Umbrella Sampling Protocol for Biomolecules. J. Chem. Phys 2008, 129, 114101–114111. [PubMed: 19044944]
44. Kirkwood JG, Statistical Mechanics of Fluid Mixtures. J. Chem. Phys 1935, 3, 300–313.
45. Kumar S; Swendsen RH; Kollman PA; Rosenberg JM, The Weighted Histogram Analysis Method for Free Energy Calculations on Biomolecules. J. Comput. Chem 1992, 13, 1011–1021.
46. Yu J; Zhou Y; Tanaka I; Yao M, Roll: A New Algorithm for the Detection of Protein Pockets and Cavities with a Rolling Probe Sphere. Bioinformatics 2010, 26, 46–52. [PubMed: 19846440]
47. van Aalten DM; Findlay JB; Amadei A; Berendsen HJ, Essential dynamics of the cellular retinol-binding protein--evidence for ligand-induced conformational changes. Protein Eng. 1995, 8, 1129–1135. [PubMed: 8819978]
48. Glykos NM, Software News and Updates. Carma: A Molecular Dynamics Analysis Program. J. Comput. Chem 2006, 27, 1765–1768. [PubMed: 16917862]
49. Ramanathan A; Agarwal PK, Computational Identification of Slow Conformational Fluctuations in Proteins. J. Phys. Chem. B 2009, 113, 16669–16680. [PubMed: 19908896]
50. Henzler-Wildman KA; Thai V; Lei M; Ott M; Wolf-Watz M; Fenn T; Pozharski E; Wilson MA; Petsko GA; Karplus M; Hubner CG; Kern D, Intrinsic Motions Along an Enzymatic Reaction Trajectory. Nature 2007, 450, 838–844. [PubMed: 18026086]
51. Kohen A, Role of Dynamics in Enzyme Catalysis: Substantial Versus Semantic Controversies. Acc. Chem. Res 2015, 48, 466–473. [PubMed: 25539442]
52. Liang FC; Kroon G; McAvoy CZ; Chi C; Wright PE; Shan SO, Conformational Dynamics of a Membrane Protein Chaperone Enables Spatially Regulated Substrate Capture and Release. Proc. Natl. Acad. Sci. U. S. A 2016, 113, E1615–1624. [PubMed: 26951662]
53. Carro J; Martinez-Julvez M; Medina M; Martinez AT; Ferreira P, Protein Dynamics Promote Hydride Tunnelling in Substrate Oxidation by Aryl-alcohol Oxidase. Phys. Chem. Chem. Phys 2017, 19, 28666–28675. [PubMed: 29043303]
54. Agarwal P; Bernard D; Bafna K; Doucet N, Enzyme Dynamics: Looking Beyond a Single Structure. ChemCatChem 2020, In Press.
55. Warshel A; Sharma PK; Kato M; Xiang Y; Liu H; Olsson MH, Electrostatic Basis for Enzyme Ccatalysis. Chem. Rev 2006, 106, 3210–3235. [PubMed: 16895325]
56. Adamczyk AJ; Cao J; Kamerlin SC; Warshel A, Catalysis by Dihydrofolate Reductase and Other Enzymes Arises from Electrostatic Preorganization, not Conformational Motions. Proc. Natl. Acad. Sci. U. S. A 2011, 108, 14115–14120. [PubMed: 21831831]
57. Fuxreiter M; Mones L, The Role of Reorganization Energy in Rational Enzyme Design. Curr. Opin. Chem. Biol 2014, 21, 34–41. [PubMed: 24769299]
58. Agarwal PK, Role of protein dynamics in reaction rate enhancement by enzymes. J. Am. Chem. Soc 2005, 127, 15248–15256. [PubMed: 16248667]
59. Smith AJ; Muller R; Toscano MD; Kast P; Hellinga HW; Hilvert D; Houk KN, Structural Reorganization and Preorganization in Enzyme Active Sites: Comparisons of Experimental and

Theoretically Ideal Active Site Geometries in the Multistep Serine Esterase Reaction Cycle. J. Am. Chem. Soc 2008, 130, 15361–15373. [PubMed: 18939839]

60. Nagel ZD; Klinman JP, A 21st Century Revisionist's View at a Turning Point in Enzymology. Nat. Chem. Biol 2009, 5, 543–550. [PubMed: 19620995]
61. Nussinov R; Ma B, Protein Dynamics and Conformational Selection in Bidirectional Signal Transduction. BMC Biol. 2012, 10, 2. [PubMed: 22277130]
62. Hammes-Schiffer S, Catalytic Efficiency of Enzymes: a Theoretical Analysis. Biochemistry 2013, 52, 2012–2020. [PubMed: 23240765]
63. Klinman JP; Kohen A, Hydrogen Tunneling links Protein Dynamics to Enzyme Catalysis. Annu. Rev. Biochem 2013, 82, 471–496. [PubMed: 23746260]
64. Klinman JP; Kohen A, Evolutionary Aspects of Enzyme Dynamics. J. Biol. Chem 2014, 289, 30205–30212. [PubMed: 25210031]
65. Otten R; Liu L; Kenner LR; Clarkson MW; Mavor D; Tawfik DS; Kern D; Fraser JS, Rescue of Conformational Dynamics in Enzyme Catalysis by Directed Evolution. Nat. Commun 2018, 9, 1314. [PubMed: 29615624]
66. Agarwal PK, A Biophysical Perspective on Enzyme Catalysis. Biochemistry 2019, 58, 438–449. [PubMed: 30507164]
67. Hou G; Zhu X; Cui Q, An Implicit Solvent Model for SCC-DFTB with Charge-Dependent Radii. J. Chem. Theory Comput 2010, 6, 2303–2314. [PubMed: 20711513]
68. Cleland WW; Hengge AC, Enzymatic Mechanisms of Phosphate and Sulfate Transfer. Chem. Rev 2006, 106, 3252–3278. [PubMed: 16895327]
69. Marcos E; Crehuet R; Anglada JM, Inductive and External Electric Field Effects in Pentacoordinated Phosphorus Compounds. J. Chem. Theory. Comput 2008, 4, 49–63. [PubMed: 26619979]
70. Marti S; Bastida A; Swiderek K, Theoretical Studies on Mechanism of Inactivation of Kanamycin A by 4'-O-Nucleotidyltransferase. Front. Chem 2018, 6, 660. [PubMed: 30761287]
71. Adams LM; Andrews RJ; Hu QH; Schmit HL; Hati S; Bhattacharyya S, Crowder-Induced Conformational Ensemble Shift in Escherichia coli Prolyl-tRNA Synthetase. Biophys. J 2019, 117, 1269–1284. [PubMed: 31542226]
72. Rajagopalan PT; Benkovic SJ, Preorganization and Protein Dynamics in Enzyme Catalysis. Chem. Rec 2002, 2, 24–36. [PubMed: 11933259]
73. Marti S; Andres J; Moliner V; Silla E; Tunon I; Bertran J, Preorganization and Reorganization as Related factors in Enzyme Catalysis: The Chorismate Mutase Case. Chemistry 2003, 9, 984–991. [PubMed: 12584715]
74. Marcus RA; Sutin N, Electron Transfers in Chemistry and Biology. Biochim. Biophys. Acta 1985, 811, 265–322.
75. Marcus RA, On the Theory of Oxidation-Reduction Reactions Involving Electron Transfer.I.. J.Phys. Chem 1956, 24, 966–978.
76. Leussing DL; Emly M, Application of Marcus Theory to Metal Ion Catalyzed Group Transfer Reactions. J. Am. Chem. Soc 1984, 106, 443–444.
77. Wladkowski BD; Brauman JI, Application of Marcus Theory to Gas-Phase SN2 Reactions: Experimental Support of the Marcus Theory Additivity Postulatef. J. Phys. Chem 1993, 97, 13158–13164.
78. Warshel A; Hwang JK; Aqvist J, Computer Simulations of Enzymatic Reactions: Examination of Linear Free-Energy Relationships and Quantum-Mechanical Corrections in the Initial Proton-Transfer Step of Carbonic Anhydrase. Faraday Discuss. 1992, 225–238. [PubMed: 1337846]
79. Marcus RA, Theoretical Relations among Rate Constants, Barriers, and Bronsted Slopes of Chemical Reactions. J. Phys. Chem 1968, 72, 891–899.
80. Grieg IR, The Analysis of Enzymic Free Energy Relationships using Kinetic and Computational Models. Chem. Soc. Rev 2010, 39, 2272–2301. [PubMed: 20419174]
81. Tu C; Qian M; Earnhardt JN; Laipis PJ; Silverman DN, Properties of Intramolecular Proton Transfer in Carbonic Aanhydrase III. Biophys. J 1998, 74, 3182–3189. [PubMed: 9635771]

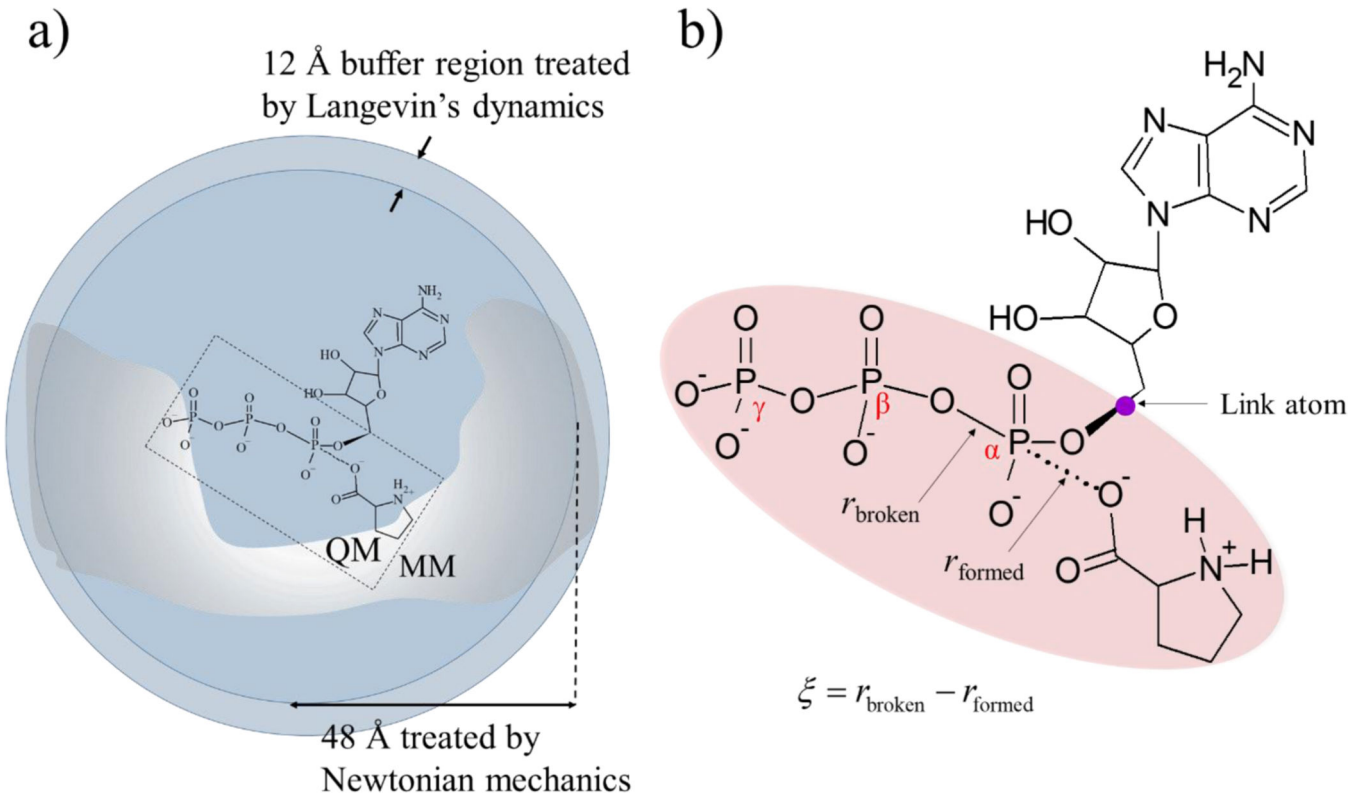

Figure 1.

Solvated protein system used for molecular dynamics simulations: a) Ef ProRS catalytic pocket with ATP and proline at the center. The QM-treated atoms, i.e., the three phosphate groups and the proline, are shown within the rectangle. All other atoms belong to the MM region, which has an outer buffer region of 12 Å treated by Langevin dynamics; b) a molecular representation (zoomed-in) of the QM-treated atoms of ATP and proline shown in red shading. The link atom separates the QM and MM-treated regions. The reaction coordinate is defined as $\xi = r_{broken} - r_{formed}$.

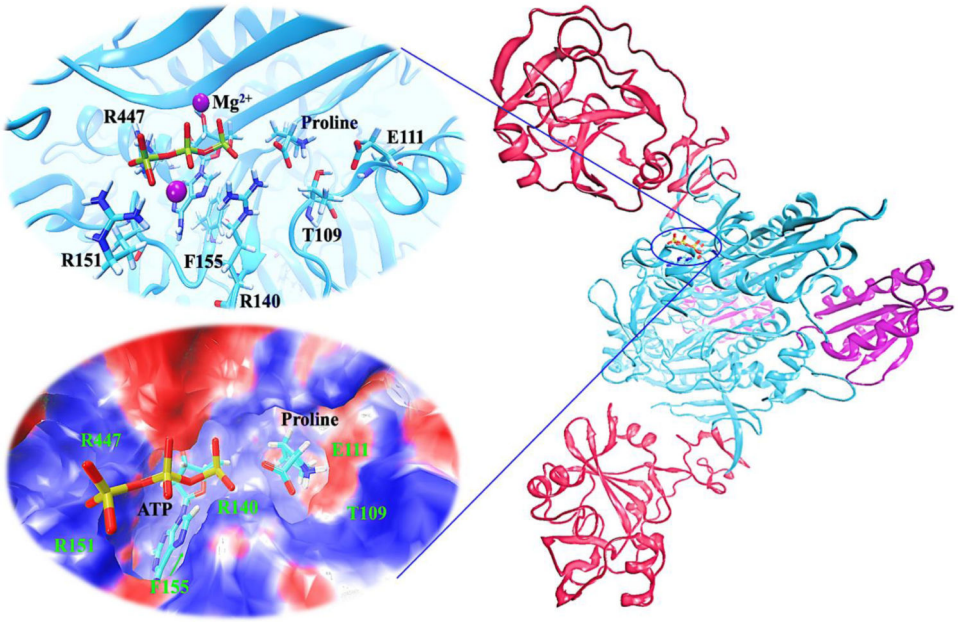

Figure 2.

The zoomed-in active site of WT Ef ProRS and the full-length protein. In the cartoon representation of the ProRS dimer (right), the editing (INS) domain is colored in red, the catalytic domain in cyan, and the anticodon-binding domain in purple. The synthetic reaction site is located in the catalytic domain, between the antiparallel β-sheet fold and the INS domain for the monomer shown on top. The key active site residues are shown in the zoomed insets. The top inset highlights the 'U-shaped' ATP and proline in the active site surrounded by several charged residues, color coded as red for negative and blue for positive in the bottom inset.

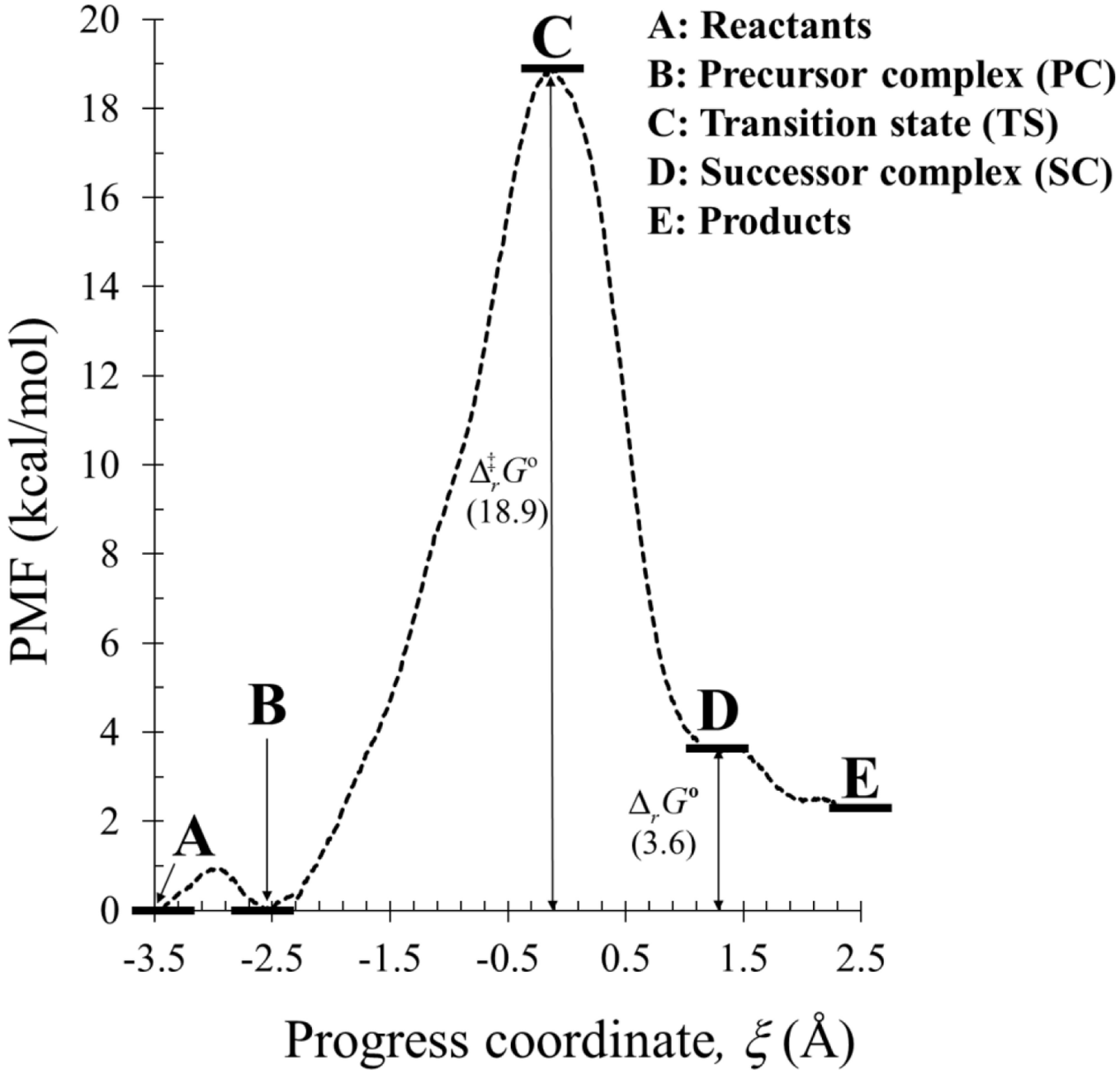

Figure 3.

The Gibbs free energy profile for prolyl-adenylate formation by WT Ef ProRS obtained from potential of mean force calculations. **A** is the reactant state, which crossed a small barrier (of ~ 1 kcal/mol of free energy) to form a local minimum that defines the precursor complexes, **B**. The transition state **C** is defined as the maximum of the free energy, while the successor complex **D** is defined by the shoulder, an inflection point on the free energy curve. After a further reduction (~ 1 kcal/mol) of free energy, the product state **E** was formed.

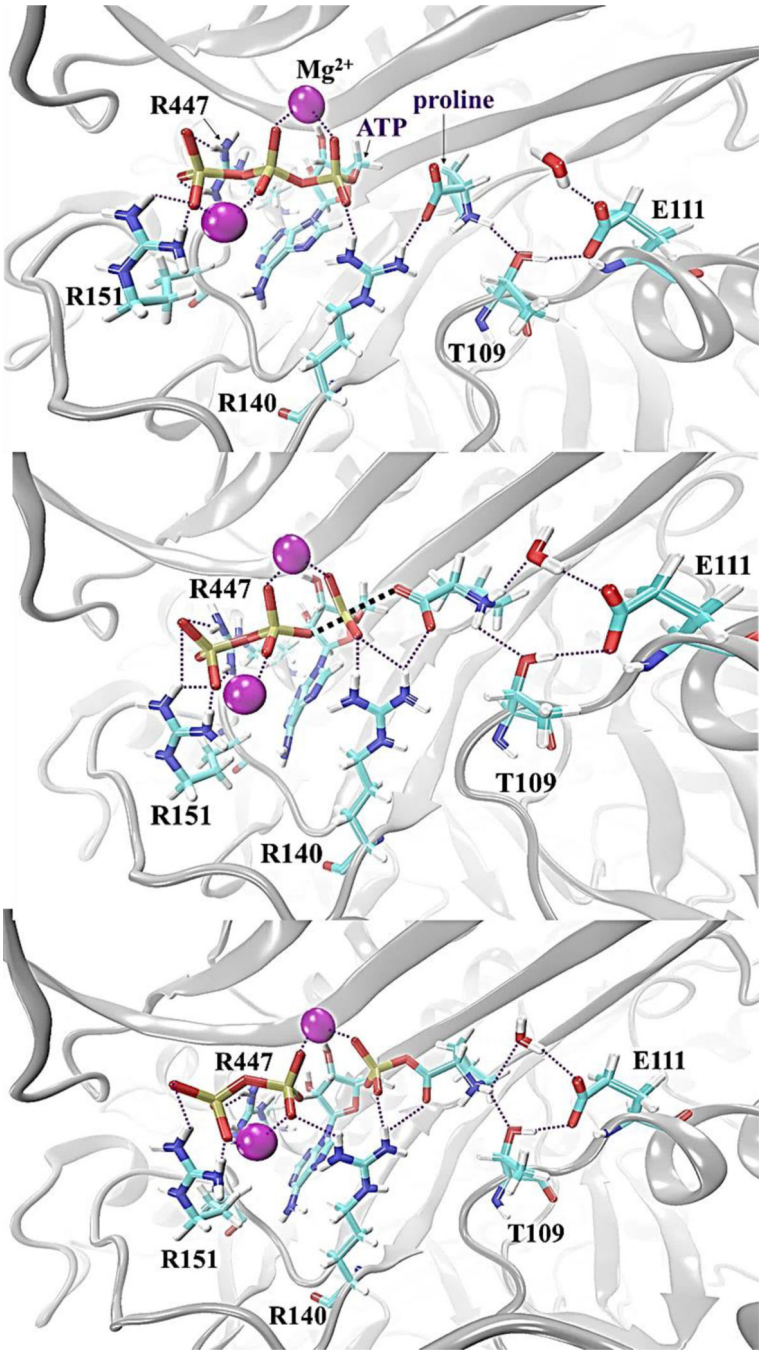

Figure 4.

Hydrogen-bond interactions at the WT Ef ProRS active site during the prolyl-adenylate formation for PC (top panel), TS (middle panel), and SC (bottom panel). The magnesium ions present in the active site are represented by purple-colored spheres.

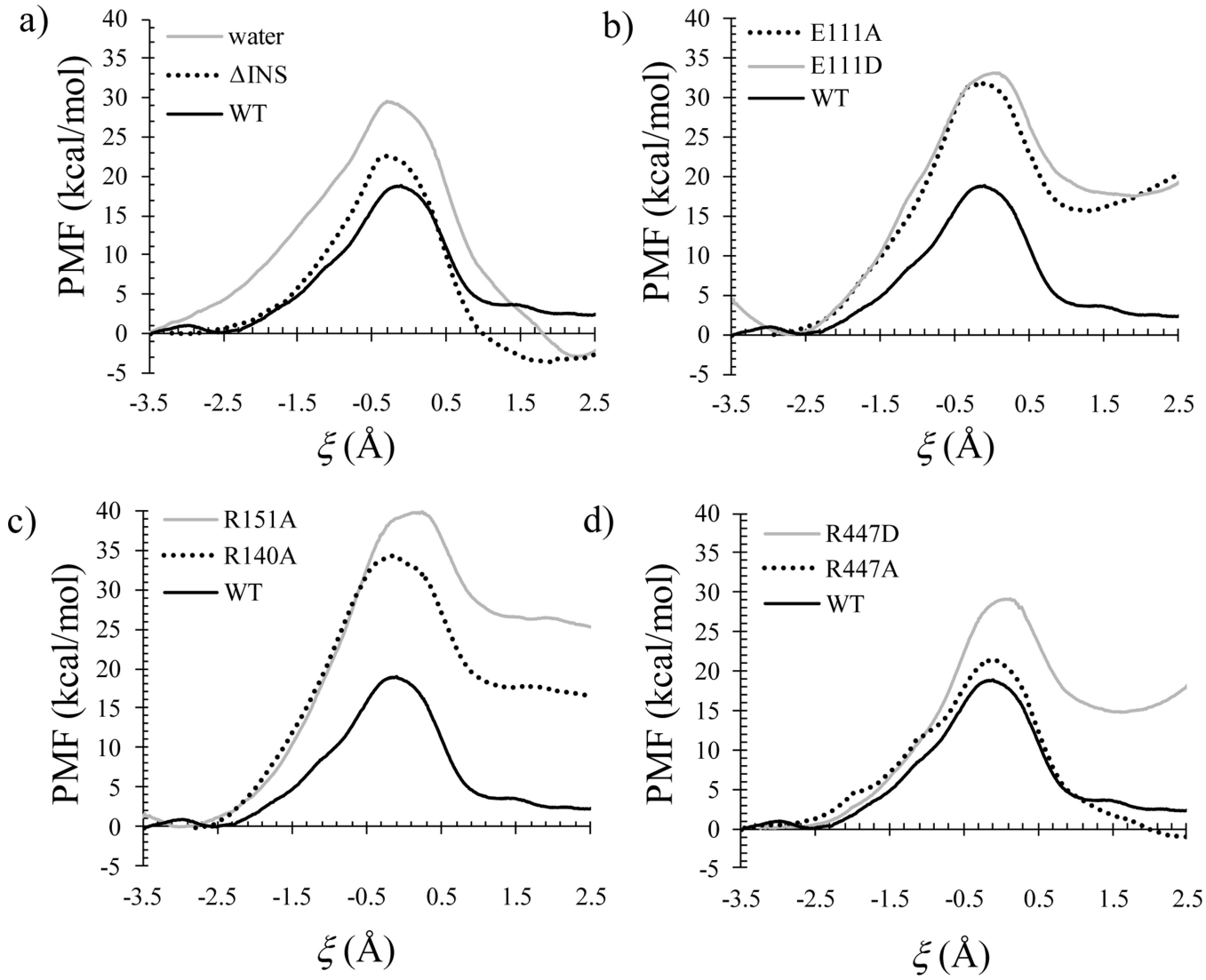

Figure 5.

The potentials of the mean force (PMF) during the prolyl-adenylate formation reaction plotted with respect to the reaction coordinate, ξ (Å): a) − d) illustrating the PMFs in aqueous, WT, and its various mutants as labelled.

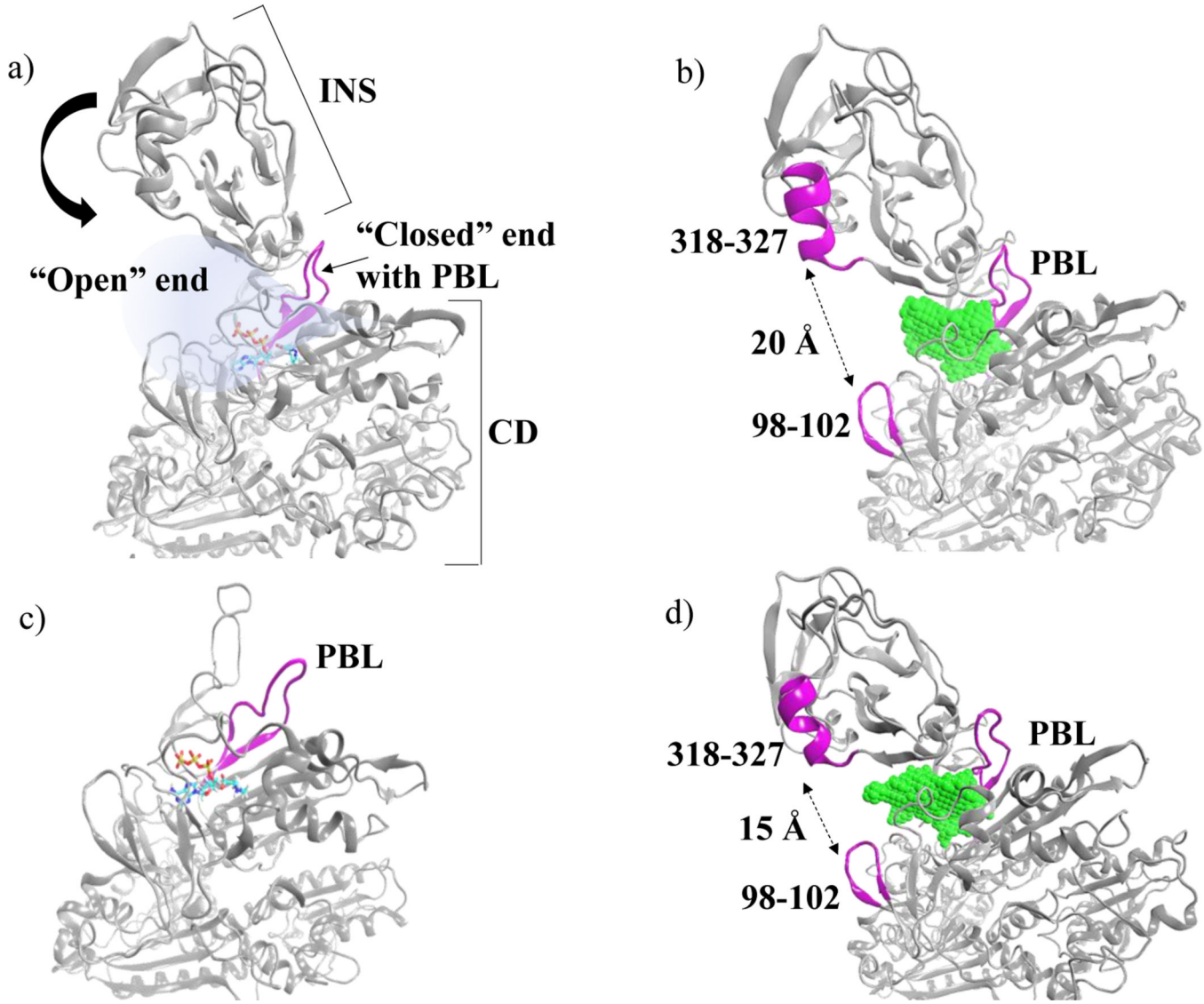

Figure 6.

Conformational changes of the INS domain during proline adenylate formation by Ef ProRS: a) the synthetic active site cleft formed at the interface of INS and CD domains is shown with blue tinge with INS positioned right above it. The cleft has the "Open" end on the left, while the other end is "Closed" by the proline-binding loop (PBL); b) the wider "Open" end of the active site cleft in the precursor complex, measured from the distance of separation of the α-helix (residues 318–327) of the INS domain (subunit A) and the loop region (residues 98–104) of the catalytic domain (subunit B), both of which are highlighted in purple. The active site volume, measured using POCASA is visually represented as clusters of green space-filling models of hydrogen atoms; c) the ΔINS mutant with the open space above the active site and the dangling PBL; d) the INS domain moves closer to the CD in the successor complex shrinking the active site as measured using the same inter-domain distance and space as in c).

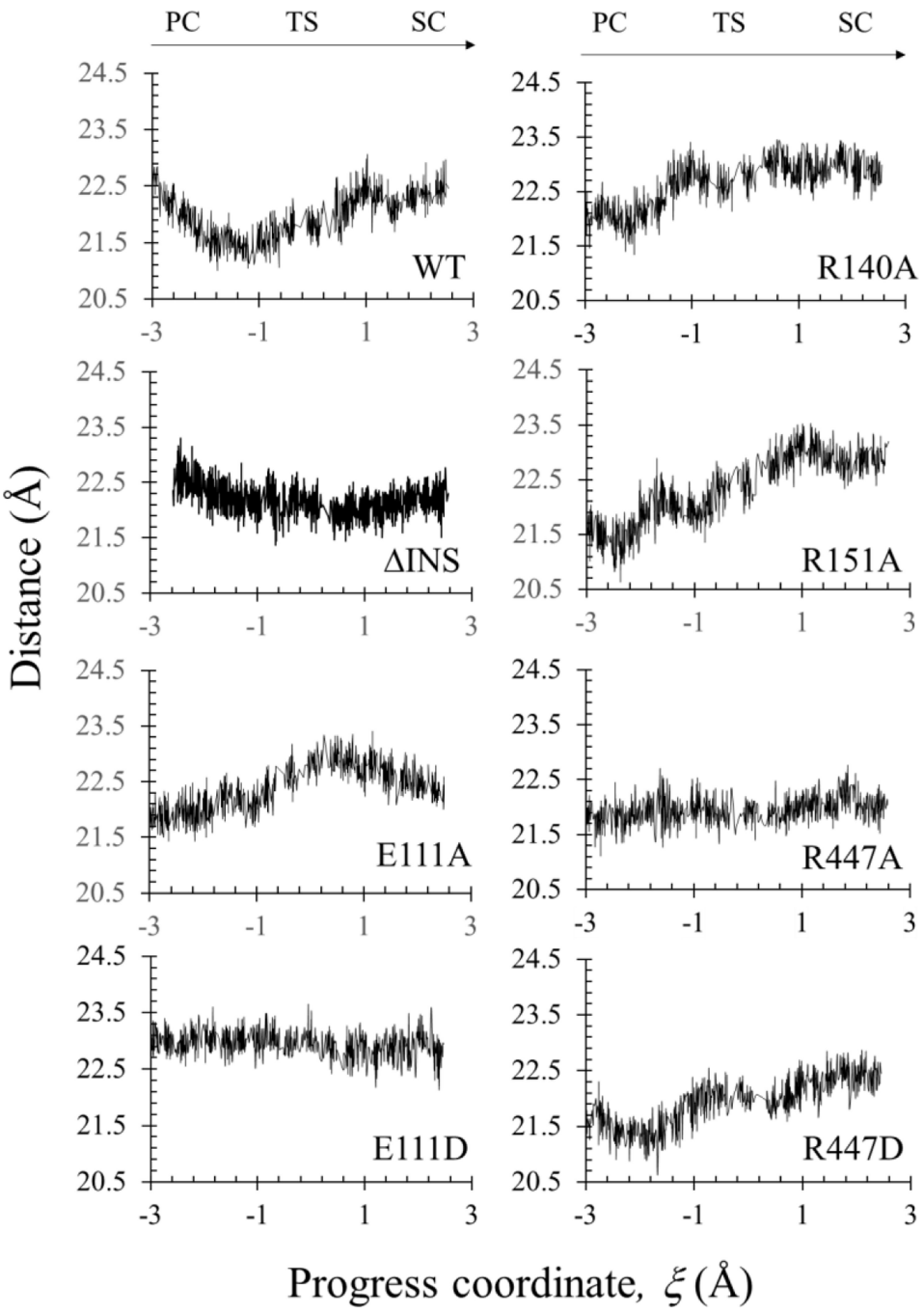

Figure 7.

Results of a 2-ns MD simulation showing the E111(C_α)-R151(C_α) distances plotted against the reaction coordinate during the catalytic reaction for WT and mutant Ef ProRS.

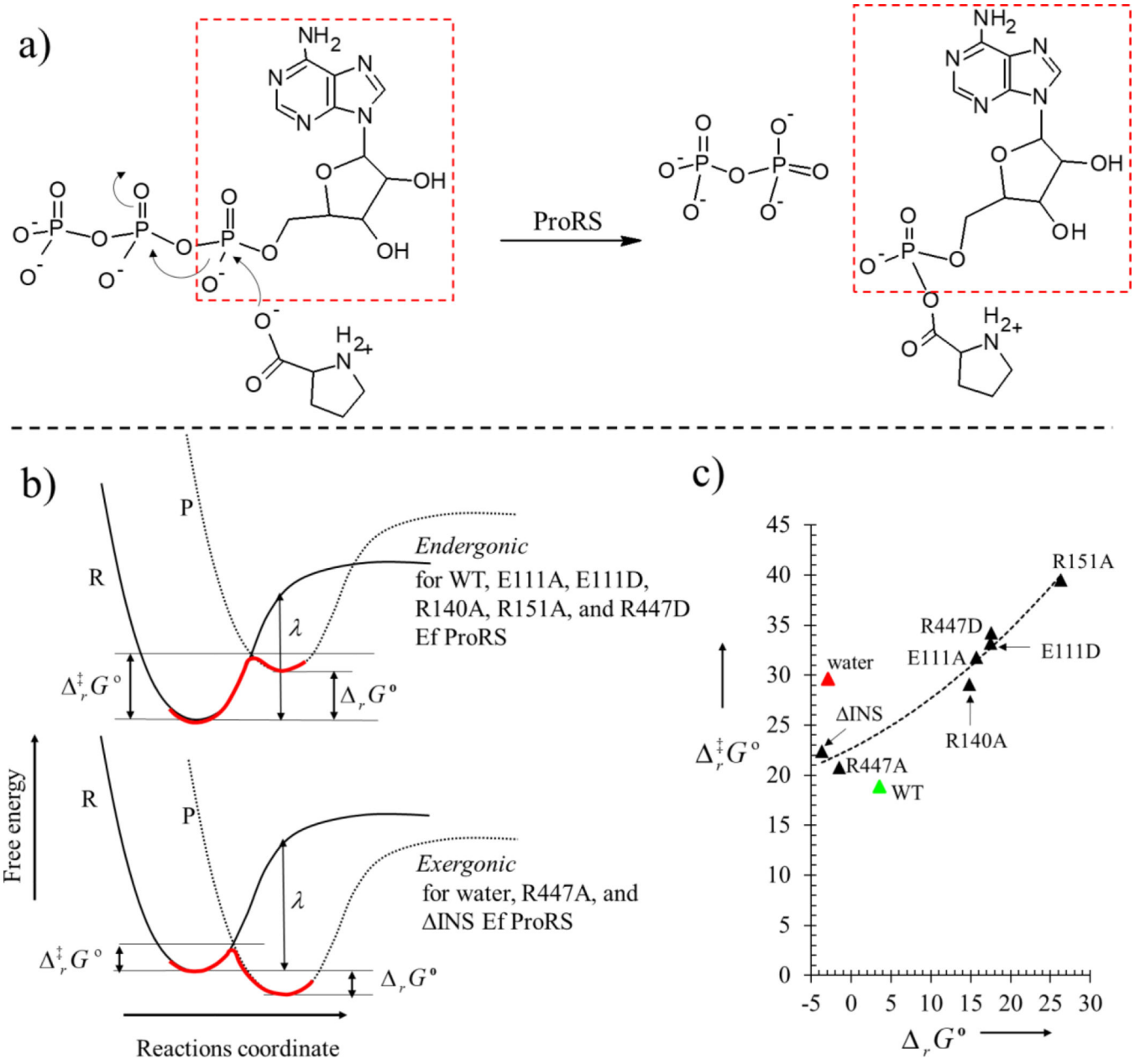

Figure 8.

Illustration of the effect of the enzyme matrix on the reorganization of the active site: a) the adenylate formation (AMP group transfer) reaction catalyzed by ProRS; b) the potential energy surfaces of reactant and product species for exergonic and endergonic reactions; the reorganization energy (λ), the Gibbs free energy of reaction ($\Delta_r G^o$), and the Gibbs free energy of activation ($\Delta_r^{\ddagger} G^o$) are labelled; c) the plot of the $\Delta_r G^o$ and $\Delta_r^{\ddagger} G^o$ for mutants (black triangles) with a fitted quadratic curve that corresponds to eq. 4 yielding a λ value of 90 kcal/mol. The λ values for the aqueous (red triangle) and WT enzyme (green triangle) systems are 117 and 61 kcal/mol, respectively.

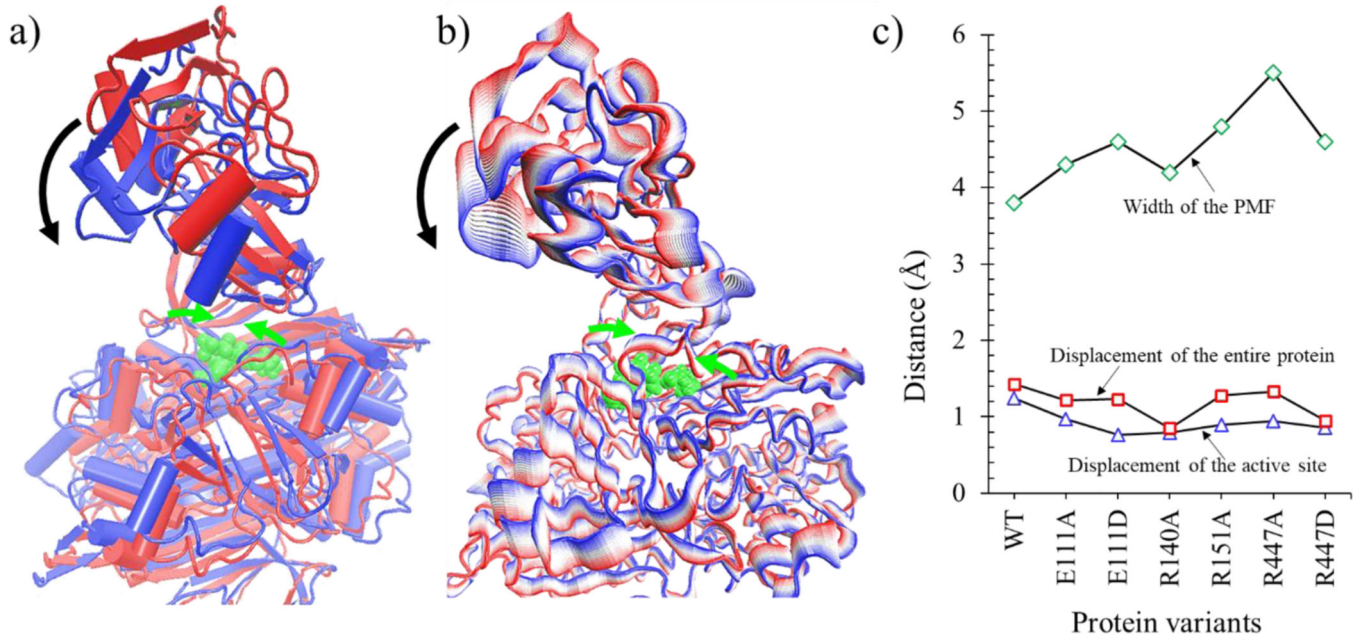

Figure 9.

The interplay of conformational dynamics and the width of the Gibbs free energy profile: a) the conformational change observed in Ef ProRS during catalysis from the MD simulation with the 'red' and 'blue' indicating the 'start' and the 'end' conformations. The preorganization dynamics of the INS domain towards the active site is shown using a single curved arrow. The reorganization compressing motion of the active site containing ATP and proline (in green vdW spheres) is illustrated by two small green arrows; b) the predominant motion along the first principal component during catalysis, with backbone and arrows shown in same colors as used in Figure 9a; c) a plot of the width of the PMF and the EDA-derived backbone (C_α atoms) displacements observed in the most populated cluster during catalysis in the WT and mutant variants. The active site consists of all C_α atoms within 20 Å of the C_α atom of the proline.

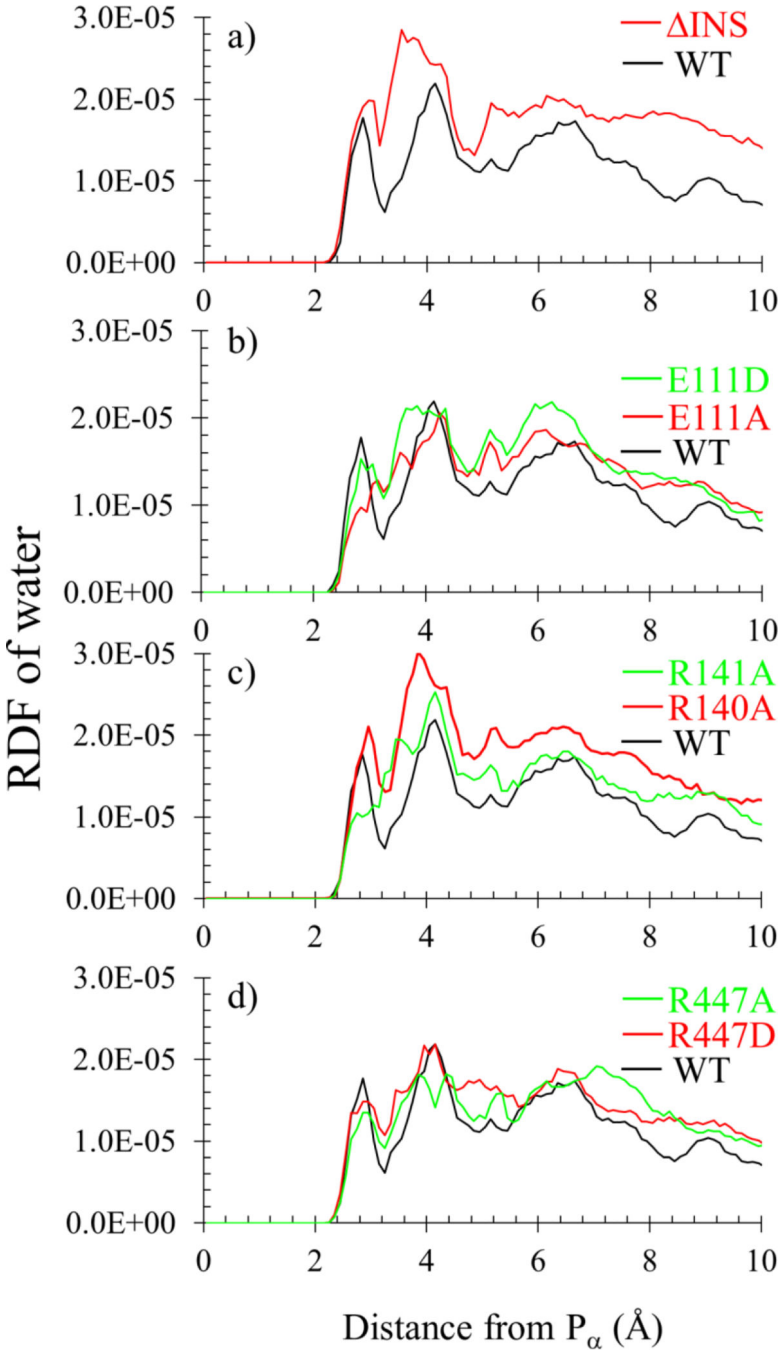

Figure 10.

The radial distribution function (RDF) of water molecules around the P_α in WT and its mutants during the catalytic prolyl-adenylate formation: a)−d) depicts the comparative RDFs for the WT and various mutants as labelled.

Table 1.

The Gibbs free energies of reaction ($\Delta_r G^o$) and activation ($\Delta_r^{\ddagger} G^o$) computed by SCC-DFTB/MM calculations for the prolyl-adenylate formation by Ef ProRS and its mutant variants. The progress of the reaction is represented by the reaction coordinate, ξ, defined as $r_{break} - r_{form}$ and illustrated in Figure 1. The generic short-hand notation for the precursor complex, the transition state, and the successor complex are PC, TS, and SC, respectively. The computed free energy quantities have an uncertainty of < 0.5 kcal/mol.

ProRS variants	ξ_{PC} (Å)	ξ_{TS} (Å)	ξ_{SC} (Å)	Width of PMF (Å)	$\Delta_r G^o$ (kcal/mol)	$\Delta_r^{\ddagger} G^o$ (kcal/mol)
WT	−2.5	−0.1	1.3	3.8	3.6	18.9
Water	< −3.5	−0.3	2.3	> 5.8	−2.9	29.6
ΔINS	−3.0	−0.3	1.9	4.9	−3.7	22.4
E111A	−3.0	−0.2	1.3	4.3	15.7	31.8
E111D	−2.7	0.0	1.9	4.6	17.5	33.2
R140A	−2.8	−0.1	1.4	4.2	17.6	34.2
R151A	−2.8	0.2	1.6	4.4	26.3	39.5
R447A	−3.0	−0.1	2.5	5.5	−1.5	20.8
R447D	−3.0	0.1	1.6	4.6	14.8	29.1

Table 2.

Catalytic efficiency of wild-type and mutant Ec ProRS for prolyl-adenylate formation. The corresponding residues in Ef ProRS are given in parenthesis.

ProRS variant	k_{cat}/K_M ($sec^{-1}mM^{-1}$)
WT	114 ± 56
ΔINS	0.24 ± 0.09
E111D	0.367 ± 0.21
E111A	Not active
R140A	Not active
R151A	Not active
R450D (R447D)	Not active
R450A (R447A)	0.236 ± 0.12

Table 3.

The predominant conformational transition, observed in the essential dynamics analysis, for the Ef ProRS WT and the mutant variants. The most populated cluster representing the first three principal components of motion was used for the substrate free state, PC state, during catalysis, and SC state. In each case, the aggregated backbone displacement was computed from the root mean square deviations (RMSD) with respect to the starting conformation in the cluster. The average displacement and its uncertainty were computed using the last 6 conformations in each case.

ProRS variants	Without ATP and proline (Å)	Precursor Complex (Å)	During Catalysis (Å)	Successor Complex (Å)
WT	3.16 ± .01	1.94 ± .01	1.43 ± .01	0.80 ± .01
E111A	2.87 ± .02	0.99 ± .01	1.22 ± .01	1.41 ± .01
E111D	2.68 ± .02	1.28 ± .01	1.23 ± .03	0.60 ± .02
R140A	4.30 ± .02	2.27 ± .01	0.85 ± .01	0.98 ± .01
R151A	2.80 ± .01	1.31 ± .01	1.28 ± .02	0.84 ± .01
R447A	3.06 ± .02	1.77 ± .01	1.33 ± .02	1.52 ± .01
R447D	2.47 ± .01	1.68 ± .01	0.95 ± .01	1.48 ±.01

Table 4.

Conformational change of Ef ProRS and its variants studied by monitoring the width of the open end of the active site cleft and the volume of the cavity. The estimated error calculated in the measurements were < 0.2 Å for the width and < 20 $Å^3$ for the volume.

ProRS variants	Precursor width (Å)	Complex volume ($Å^3$)	Successor width (Å)	Complex volume ($Å^3$)
WT	19.7	1110	14.5	1044
E111A	17.0	1109	13.2	1067
E111D	13.1	1287	10.9	977
R140A	19.0	1569	14.2	927
R151A	19.5	1104	14.5	995
R447A	18.5	1127	16.4	1524
R447D	16.0	1163	11.9	1091